QoS-Aware Precoder Optimization for Radar Sensing and Multiuser Communications Under Per-Antenna Power Constraints

Chao Wang, *Senior Member, IEEE*, Zan Li, *Senior Member, IEEE*, Naofal Al-Dhahir, *Fellow, IEEE*,

Kyeong Jin Kim, *Senior Member, IEEE*, and Kai-Kit Wong, *Fellow, IEEE*

Abstract—In this work, we concentrate on designing the precoder for the multiple-input multiple-output (MIMO) dual functional radar-communication (DFRC) system, where the dual-functional waveform is designed for performing multiuser downlink transmission and radar sensing simultaneously. Specifically, considering the signal-independent interference and signal-dependent clutter, we investigate the optimization of transmit precoding for maximizing the sensing signal-to-interference-plus-noise ratio (SINR) at the radar receiver under the constraint of the minimum SINR received at multiple communication users and per-antenna power budget. The formulated problem is challenging to solve due to the nonconvex objective function and nonconvex per-antenna power constraint. In particular, for the signal-independent interference case, we propose a distance-majorization induced algorithm to approximate the nonconvex problem as a sequence of convex problems whose optima can be obtained in closed form. Subsequently, our complexity analysis shows that our proposed algorithm has a much lower computational complexity than the widely-adopted semidefinite relaxation (SDR)-based algorithm. For the signal-dependent clutter case, we employ the fractional programming to transform the nonconvex problem into a sequence of subproblems, and then we propose a distance-majorization based algorithm to obtain the solution of each subproblem in closed form. Finally, simulation results confirm the performance superiority of our proposed algorithms when compared with the SDR-based approach. In conclusion, the novelty of this work is to propose an efficient algorithm for handling the typical problem in designing the DFRC precoder, which achieves better performance with a much lower complexity than the state-of-the-art algorithm.

Index Terms—Dual-functional radar-communication, radar sensing, transmit precoding, signal-independent interference, signal-dependent clutter,

I. INTRODUCTION

Wireless communications and radar sensing have developed in parallel for decades. Although there are many commonalities in their signal processing approaches and signal waveforms, their developments have had limited intersections.

C. Wang and Z. Li are both with the Integrated Service Networks Lab, Xidian University, Xi'an 710071, China. (e-mail: drchaowang@126.com, zanli@xidian.edu.cn).

N. Al-Dhahir is with the Department of Electrical and Computer Engineering, the University of Texas at Dallas, Richardson, TX 75080 USA (e-mail: aldhahir@utdallas.edu).

Kyeong Jin Kim is with Mitsubishi Electric Research Laboratories (MERL), Cambridge, MA 02139 USA (e-mail:kyeong.j.kim@hotmail.com).

K.-K. Wong is with the Department of Electronic and Electrical Engineering, University College London, London WC1E 6BT, U.K. (e-mail: kai-kit.wong@ucl.ac.uk).

However, as wireless communications research progresses towards 5G-Advanced and 6G wireless networks, robust sensing functionality as well as reliable wireless connectivity are both regarded as important features, especially for location-aware services [1], [2]. Accordingly, the research on integrated sensing and communication (ISAC) has received increasing attention in recent years [3]–[5].

Generally speaking, the research on ISAC has been conducted in two main directions, i.e., the coexistence of radar and communication (CRC) and dual functional radar-communication (DFRC). CRC focuses on efficient management of the mutual interference between radar sensing and wireless communications [6], [7] and it dates back to 1960s [8]. To maximize the efficiency of coexistence, the CRC time allocation was studied in [9]. The work of [10] presented a spectral co-design for a statistical multiple-input multiple-output (MIMO) radar and full-duplex multiuser MIMO communications. In [11], a distributed beamforming design approach was proposed for a joint distributed radar-communications coexisting system. Employing multicarrier waveforms, the authors of [12] considered the power allocation design for handling the CRC spectrum sharing problem in cluttered environments. By exploring constructive interference, the work of [13] proposed a novel CRC coexistence mechanisms. The energy efficiency optimization of the coexistence of multiple-input multiple-output (MIMO) communications and surveillance radar was considered in [14]. Different from CRC, DFRC concentrates on designing a common signal waveform on the same hardware platform for realizing radar sensing and communications simultaneously [3], [4]. The key technical challenge of DFRC is how to design a common waveform to achieve the two functionalities of sensing and communications simultaneously.

The authors of [4] pointed out that DFRC research can be broadly divided into three directions: radar-centric design, communication-centric design, and joint design. In radar-centric design, the communication signal is embedded in radar pulses. For example, the work of [15] employed linear frequency modulated (LFM) signaling to integrate a simple search radar and digital communications function. The work of [16] adopted a multi-objective optimization algorithm to design an integrative waveform for intrapulse radar-embedded communications. Besides, the authors of [17] proposed a new frequency modulation (FM) scheme for embedding commu-

nication signals into radar waveforms under the constraint of constant envelope constraint.

Communication-centric designs use the communication waveform to realize radar-sensing functionality whose design priority is still on communications. Such a design philosophy of building perceptive mobile networks with the added radar sensing is attractive and actively investigated [18], [19]. The seminal work of [20] studied the design of communication waveforms, which can perform data transmission and radar sensing simultaneously. After that, the study on the communication-centric designs received the increasing attentions [19]. Considering MIMO DFRC systems, the authors of [18] employed the symbol-level precoding approach to design the transmit signal waveform for radar sensing and multiuser broadcasting. In [21], the authors jointly employed the space-time adaptive processing and symbol-level precoding approaches to design the signal waveform and receiving filter for maximizing radar sensing signal-to-interference-plus-noise ratio (SINR) under the constraints of communication quality-of-service (QoS) and waveform. Considering that the radar target may be a potential eavesdropper, the authors of [22] proposed to design the transmit waveform for maximizing the SINR of the radar under the physical layer security constraint. The work in [23] further considered the joint optimization of communication signal and artificial noise for securing wireless communications and guaranteeing radar sensing performance.

The joint designs separated the waveform optimization from existing communication and radar standards and offered a trade-off between radar sensing and communications [24]. The advanced development of multi-antenna technology has provided sufficient spatial degrees-of-freedom (DoF) to wireless communications, especially for massive MIMO, which provided another design approach for the joint design in the spatial domain [4]. The work in [25] proposed MIMO DFRC beamforming designs for minimizing the Cramér-Rao bound while guaranteeing communication QoS constraints. Adopting the weighted sum of multi-user interference, waveform similarity, and integrated sidelobe level as the objective function, the work in [26] investigated the DFRC waveform design for balancing the performance of communications and radar sensing. The authors of [27] proposed several approaches for investigating the optimal design of DFRC waveform under radar-specific constraints. Furthermore, the authors of [28] proposed a constructive interference based precoder optimization approach to design the waveform for achieving a favorable trade-off between radar and communications. In [29], a Pareto optimization framework was proposed for MIMO DFRC, with an achievable radar-communication performance region.

However, the works mentioned above all adopted the symbol-level precoding to design the instantaneous DFRC waveform, whose computational complexity is high when considering the time-varying feature of communication signals [30]. To realize a low-complexity design, several works resorted to design the transmit precoder by making the average covariance satisfy the radar sensing performance. For instance, the work of [30] proposed to adopt the weighted sum of radar waveform and communication signals for achieving DFRC functionality and a semidefinite relaxation (SDR)-based algo-

rithm is proposed to design the precoders of communication symbols and radar waveform. Subsequently, the authors of [31] fixed the covariance of the transmit waveform as the optimal radar waveform for guaranteeing radar sensing performance and optimized the transmit precoders of communication signals and radar waveform for balancing the SINR received at multiple communication users. Besides, the work of [32] adopted the rate-splitting multiple access technique to split the message into a radar sequence and communication signals and designed their precoders for achieving DFRC functionality. Moreover, the work of [33] proposed to adopt non-orthogonal multiple access to design a novel double spectrum sharing strategy for facilitating the system design of joint radar and multicast-unicast communications. In addition, the authors of [34] developed an integrated communication, radar sensing, and mobile-edge computing architecture, which jointly considered the radar sensing, multiuser broadcasting, and computation offloading energy consumption and the authors built a multi-objective optimization problem to perform the resource allocation. In conclusion, the added radar probing signals not only increase the available spatial DoF, but also facilitate the precoder design [30], [31]. However, it is worth noting that the added probing signals exclusive to radar sensing will increase the interference of wireless networks and degrade the network performance. From the perspective of network interference management, it is better to only transmit communication signals and optimize the communication precoder for achieving the DFRC functionality [35]. Following this idea and considering MIMO radar and multiuser MIMO communications, the authors of [36] adopted the successive convex approximation (SCA) approach to design the precoder of communication signals for achieving radar sensing and multiuser broadcasting. Considering the issues of hybrid transmit beamforming design and direction-of-arrival estimation in multi-carrier DFRC systems, the authors of [37] proposed a consensus alternating direction method of multipliers framework for handling the resulting nonconvex optimization problem. Besides, the authors of [38] considered the beamforming optimization of a DFRC BS, where the energy efficiency of the multiuser communication is maximized under the constraints of radar sensing performance. The work in [39] studied the limited feedforward waveform design for orthogonal frequency division multiplexing (OFDM) DFRC systems, which considers both the minimization of the Cramér-Rao bound on delay-Doppler estimation and the maximization of the communications rate under radar similarity constraint. Considering full-duplex communications for DFRC, the authors of [40] studied the joint optimization of the downlink dual-functional transmit signal, the uplink receive beamformers at the BS, and the transmit power at the uplink users. The work in [41] studied the precoder design for MIMO DFRC systems, where radar and communication modes use distinct baseband waveforms and the corresponding precoders are optimized for spatial multiplexing. The novelty of our work is boldly and explicitly contrasted to the open literature in Table-I

Nevertheless, the DFRC precoder optimization problem is nonconvex in most cases. For handling this challenging problem, the works mentioned above adopted SDR or SCA-

TABLE I
OVERVIEW OF EXISTING LITERATURE

Feautures	Proposed	[35]	[14]	[7]	[39]	[40]	[41]	[11]	[10]	[29]	[22]	[25]
DFRC System Design	✓	✓			✓	✓	✓			✓	✓	✓
OFDM Waveform		✓		✓	✓							
Multiuser Interference	✓			✓		✓	✓	✓	✓	✓		✓
SDR-Based Approach						✓	✓					✓
Radar Waveform Constraints	✓				✓		✓		✓	✓		
Dedicated Radar Signal			✓	✓		✓	✓	✓	✓			✓
Signal Covariance Design			✓							✓		
Sensing SINR Maximization	✓	✓		✓								
Broadcast Communications	✓	✓				✓	✓	✓	✓	✓		✓
Spectrum Sharings			✓	✓				✓	✓			
Uplink Communications						✓		✓	✓			
Clutter Interference	✓	✓	✓								✓	
Physical Layer Security											✓	

based algorithms to approximate the nonconvex problem as a sequence of convex problems to locate a suboptimal solution. However, SDR-based algorithms lift the dimension of optimization variables that increases the computational complexity. In addition, the SCA-based algorithm needs a feasible solution to enable the iterative algorithm, but a feasible solution is also very difficult to obtain. Until now, there is still a lack of an efficient algorithm for handling the nonconvex optimization problem.

Against this background, this work proposes a distance-majorization [42] induced low-complexity algorithm for handling the DFRC precoder design. In our considered DFRC system, a dual-functional base station (BS) performs radar sensing to detect the targets in the presence of interference and acts as a wireless broadcast transmitter to serve multiple downlink users. Considering the signal-independent interference [36], [43], [44] and signal-dependent clutter [45], [46] respectively, we investigate the precoder optimization problem to maximize the sensing SINR of the radar under the constraints of the minimum SINR received at multiple communication users and per-antenna power budget. In particular, by employing the distance-majorization algorithm, we approximate the considered problem as a sequence of unconstrained convex problems whose analytical solutions can be obtained in closed form. Accordingly, we can derive a low-complexity DFRC precoder optimization algorithm. The key challenges lie in reformulating the complex-domain optimization problem as its real counterpart and obtaining the closed-form solution of the subproblem at each iteration. Besides, it is also challenging to establish the convergence of our proposed distance-majorization algorithm to Karush-Kuhn-Tucker (KKT) solutions of the original nonconvex problem due to the problem reformulation. Our main contributions are summarized as follows.

1) Considering the signal-independent interference, we adopt the distance-majorization algorithm to incorporate the minimum received SINR constraint and per-antenna power budget into the objective function. Then, the constrained nonconvex optimization problem is approximated

as a sequence of unconstrained convex problems. Moreover, we prove that the approximate problem has the same optimal solution as the original problem. Subsequently, we obtain the analytical solution of each subproblem in closed form through exploiting the Karush-Kuhn-Tucker (KKT) conditions, which bypasses the need of implementing the interior point method to handle an optimization problem and obtains a low-complexity design.

2) Considering the signal-dependent clutter, the precoder design is a nonconvex optimization problem due to the nonconvex objective function and constraints. We adopt the fractional programming approach [47] for transforming the nonconvex objective function into a multivariate function that facilitates solving the problem. This is because the obtained multivariate function is a convex function of any variable when fixing the other ones. Then, we propose an alternating optimization algorithm to solve the problem iteratively. For handling the subproblem during the iteration, we propose a distance-majorization induced algorithm to solve it in closed form.

3) Our computational complexity analysis shows that our proposed distance-majorization induced algorithm has a much lower complexity than the SDR-based algorithm. Moreover, for the signal-independent interference case, our numerical results show that compared with the SDR-based algorithm, our proposed algorithm not only arrives at a better radar beampattern with larger power gains at the target directions and lower nulling beamformer at the interfering directions, but also acquires a larger radar sensing SINR.

4) Considering the tracking scenario, the performance of our proposed precoder design approach has been validated by numerical results. Specifically, we design the DFRC precoder with the imperfect angle estimation obtained by the extended Kalman filter (EKF)-based tracking filter, which can guarantee a very reliable target tracking performance in the presence of signal-independent interference and signal-dependent clutter.

Notation: $\otimes$, $(\cdot)^T$, $(\cdot)^H$, $||\cdot||_*$, $||\cdot||_2$, and $||\cdot||_F$ denote
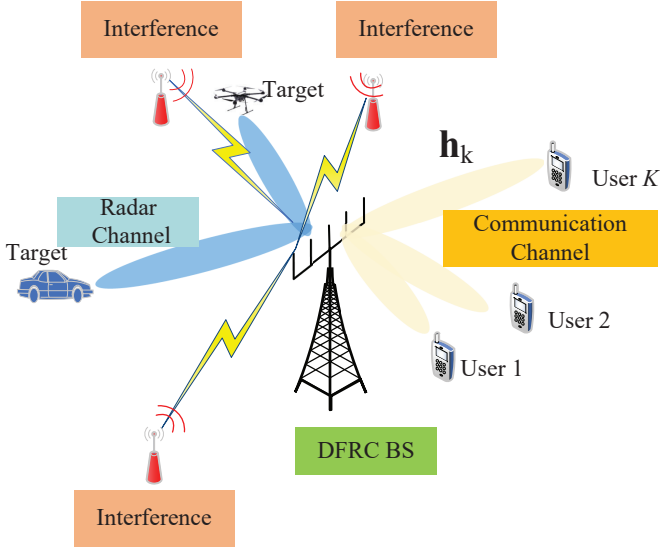
Fig. 1. Illustration of the considered MIMO-DFRC system.

the Kronecker product, the transpose, the conjugate transpose, the nuclear norm, the L_2 norm, and the Frobenius norm of a matrix, respectively; $\mathrm{Tr}\,(\cdot)$ and $(\cdot)^{-1}$ denote the trace and the inverse of a square matrix, respectively; $\mathbb{C}^{n \times n}$ stands for an $n \times n$ complex matrix and $\mathbb{S}_+^N$ denotes the set of Hermitian positive semi-definite $N \times N$ matrices; $\mathbf{x} \sim \mathcal{CN}\,(\mathbf{\Lambda}, \mathbf{\Delta})$ denotes the circularly symmetric complex Gaussian vector having a mean vector of $\mathbf{\Lambda}$ and covariance matrix of $\mathbf{\Delta}$. $\mathbf{I}_N$ is the $N \times N$ identity matrix. $\mathbb{E}(\cdot)$ is the expectation operator. $\mathrm{Diag}\,(\mathbf{a}_1, \ldots, \mathbf{a}_N)$ denotes a block diagonal matrix where $\mathbf{a}_1, \ldots, \mathbf{a}_N$ are the main-diagonal blocks. $\mathcal{R}(a)$ and $\mathcal{I}(a)$ denote the real and imaginary parts of a complex number a, respectively. $O\,(\cdot)$ is the big-O notation. $\nabla\,(\cdot)$ denotes the gradient operator.

II. SYSTEM MODEL

As illustrated in Fig. 1, this work studies a MIMO DFRC system, where a multi-antenna BS serves K users in the downlink broadcast channel while performing radar sensing. The dual functional radar-communication is achieved by designing the transmit waveform. Following [36], [48], we only adopt the communication waveform to perform radar sensing, since such an assumption requires minimal changes in existing wireless communication systems and does not introduce extra interference to wireless networks. Assuming that the BS is equipped with N_t transmit antennas and N_R receive antennas, we denote the transmitted signal in L time-slots as

$$\mathbf{x} = \mathbf{W}\mathbf{s}, \qquad (1)$$

where the digital baseband precoder is defined by $\mathbf{W} \in \mathbb{C}^{N_t \times K}$ and the communication signal $\mathbf{s} \triangleq \left[\mathbf{s}^T(1), \ldots, \mathbf{s}^T(L)\right]^T \in \mathbb{C}^{K \times L}$. In addition, following [30], [31], [49], the communication signals intended to different users are assumed to be uncorrelated, i.e., $\mathbb{E}\left(\mathbf{s}\mathbf{s}^H\right) = \mathbf{I}_K$.

The objective of this work is to study the optimization of the precoder $\mathbf{W}$ for maximizing the radar sensing performance subject to multiple users' individual quality of service (QoS) constraints.

A. Multiuser Communication Performance

With the transmit signal $\mathbf{x}$ given in (1), the signal $\mathbf{y}_k$ received at the kth user can be derived as

$$
\begin{aligned}
\mathbf{y}_k &= \mathbf{h}_k^H \mathbf{x} + \mathbf{n}_k \\
&= \mathbf{h}_k^H \mathbf{W}(:,k)\mathbf{s}(k,:) + \underbrace{\sum_{j \neq k} \mathbf{h}_k^H \mathbf{W}(:,j)\mathbf{s}(j,:)}_{\text{Mutual Interference}} + n_k, \quad (2)
\end{aligned}
$$

where $\mathbf{W}(:,k)$ is the kth column of $\mathbf{W}$ and $\mathbf{s}(k,:)$ is the kth row of $\mathbf{s}$. Besides, $\mathbf{h}_k^H \in \mathbb{C}^{1 \times N_t}$ is the downlink Rayleigh fading channel from the BS to the kth user whose elements are assumed to follow $\mathcal{CN}\,(0,1)$ and $n_k \sim \mathcal{CN}(0, \sigma_c^2)$ is the received noise.

Based on the assumptions above, the receiver SINR at the kth user is given by

$$\varrho_{c,i}\,(\mathbf{W}) \triangleq \frac{|\mathbf{h}_i^H \mathbf{W}(:,i)|^2}{\sum_{j \neq i} \mathbf{h}_i^H \mathbf{W}(:,j)\,(\mathbf{W}(:,j))^H\,\mathbf{h}_i + \sigma_c^2}. \qquad (3)$$

B. MIMO Radar Sensing Performance

The signal received at the radar receiver is given by

$$x_0 = \mathbf{t}^H \mathbf{y}_0 = \mathbf{t}^H \mathbf{A}(v)\mathbf{W}\mathbf{s} + \mathbf{t}^H \mathbf{c} + \mathbf{t}^H \mathbf{z}_0, \qquad (4)$$

where $\mathbf{t}$ is the linear receive filter adopted at the radar, α_i is the ith target radar cross section, $\mathbf{A}(v) = \sum_{1 \leq i \leq M} \alpha_i \boldsymbol{\alpha}_r(v_i)\boldsymbol{\alpha}_t^T(v_i)$, where M is the number of targets, $\mathbf{a}_t(v_i) = \left[1, \ldots, e^{-j2\pi(N_t-1)\Delta_t \sin(v_i)}\right]^T$, and $\mathbf{a}_r(v_i) = \left[1, \ldots, e^{-j2\pi(N_r-1)\Delta_r \sin(v_i)}\right]^T$ are respectively the steering vectors for the receive and transmit signals. In addition, Δ_t and Δ_r are antenna elements separation distances normalized by the wave length, $\mathbf{z}_0 = \left[\mathbf{z}_0^T(1), \ldots, \mathbf{z}_0^T(L)\right]^T$ is the received noise, and $\mathbf{z}_0(l) \sim \mathcal{CN}\left(\mathbf{0}, \sigma_r^2 \mathbf{I}_{N_r}\right)$. Besides, $\mathbf{c} \triangleq \left[\mathbf{c}^T(1), \ldots, \mathbf{c}^T(L)\right]^T \in \mathbb{C}^{N_r \times L}$ denotes the received interference which can be modeled as signal-independent interference [36], [43], [44] or signal-dependent clutter [45], [46].

This paper considers the radar tracking scenario to design the DFRC precoders, where the number and angles of the targets can be acquired in the radar search mode to enable target tracking. Besides, the number and angles of the targets can also be regarded as the directions of interest needed to sensing, where the DFRC base station (BS) emits signals to detect potential targets in M spatial directions. Therefore, following existing works on DFRC, e.g., [18], [21]–[36], we assume that the number and angles of the targets are available and the output SINR of the radar can be calculated as [36], [43], [45]

$$\omega\,(\mathbf{t}, \mathbf{W}) = \frac{\mathbf{t}^H \mathbf{A}(v)\mathbf{W}\mathbf{s}\mathbf{s}^H \mathbf{W}^H \mathbf{A}^H(v)\mathbf{t}}{\mathbf{t}^H \mathbf{c}\mathbf{c}^H \mathbf{t} + \mathbf{t}^H \mathbf{z}_0 \mathbf{z}_0^H \mathbf{t}}. \qquad (5)$$

As shown in [45], the optimal $\mathbf{t}^*$ is the solution of minimum variance distortionless response (MVDR) problem solution, given by

$$\mathbf{t}^* = \frac{\left(\mathbf{cc}^H + \mathbf{z}_0\mathbf{z}_0^H\right)^{-1}\mathbf{A}(\upsilon)\mathbf{Ws}}{\mathbf{s}^H\mathbf{W}^H\mathbf{A}(\upsilon)^H\left(\mathbf{cc}^H + \mathbf{z}_0\mathbf{z}_0^H\right)^{-1}\mathbf{A}(\upsilon)\mathbf{Ws}}. \quad (6)$$

Then, substituting (6) into (5), the output SINR of the radar can be calculated as

$$\begin{aligned}
\bar{\omega}(\mathbf{W}) &= \mathrm{Tr}\left(\mathbf{s}^H\mathbf{W}^H\mathbf{A}^H(\upsilon)\left(\mathbf{cc}^H + \mathbf{z}_0\mathbf{z}_0^H\right)^{-1}\mathbf{A}(\upsilon)\mathbf{Ws}\right) \\
&= \mathrm{Tr}\left(\frac{\mathbf{ss}^H}{L}\mathbf{W}^H\mathbf{A}^H(\upsilon)\left(\frac{\mathbf{cc}^H}{L} + \frac{\mathbf{z}_0\mathbf{z}_0^H}{L}\right)^{-1}\mathbf{A}(\upsilon)\mathbf{W}\right) \\
&\overset{(a)}{\approx} \mathrm{Tr}\left(\mathbf{\Theta}\mathbf{W}\mathbf{W}^H\right), \quad (7)
\end{aligned}$$

where $\mathbf{\Theta} \triangleq \mathbf{A}^H(\upsilon)\left(\mathbf{R}_c + \sigma_c^2\mathbf{I}_{N_r}\right)^{-1}\mathbf{A}(\upsilon)$. In addition, step (a) holds asymptotically for a sufficiently large L [25], [31], since $\mathbb{E}\left(\mathbf{ss}^H\right) = \mathbf{I}_K$ and $\mathbf{c}(i) \sim \mathcal{C}\left(\mathbf{0}, \mathbf{R}_c\right)$. The accuracy of such an asymptotic result has been validated by simulation results in [31, Section VII-F and VII-G].

We formulate the precoder design problem as the following constrained optimization problem, which maximizes the SINR of the MIMO radar under the minimal SINR received at each user and per-antenna power constraint, i.e.,

$$\max_{\mathbf{W}} \mathrm{Tr}\left(\mathbf{\Theta}\mathbf{W}\mathbf{W}^H\right) \quad (8a)$$

$$\text{s.t.} \quad \varrho_{c,i} \geq R_i, \forall i \in \{1, \ldots, K\} \quad (8b)$$

$$\mathrm{diag}\left(\mathbf{W}\mathbf{W}^H\right) = \frac{P_{\mathrm{tot}}}{N_t}\mathbf{I}, \quad (8c)$$

where R_i is the SINR constraint of the ith user. Besides, we adopt the constant per-antenna power constraint, since the radar needs a per-antenna power control for transmitting the signal with maximal power budget [18], [26], [30].

Problem (8) is nonconvex due to the nonconvexity of the objective function and constraint (8c). For handling problem (8), traditional methods reformulate it as the rank-constrained SDP [30]. However, different from [30, Theorem 1], the rank-1 solution of problem (8) does not always exist due to the absence of the dedicated beamforming matrix for radar waveforms. Therefore, when applying the SDR algorithm, extra work is needed to reconstruct a rank-1 solution, e.g., using the Gaussian randomization method [50] and penalty-based approach [33], whose complexity is high. We adopt the penalty-based algorithm as the benchmark to perform the performance comparison, whose details are given in Appendix C. As an alternative, this work employs the distance-majorization induced algorithm [42] to propose a low-complexity joint design algorithm, which adopts the deviation of the solution from the feasible region as the penalty to transform the nonconvex optimization problem into a sequence of unconstrained problems whose solutions can be derived in closed-form.

In the following, we first consider the signal-independent (exogenous) interference including interference from other radiators [44] to investigate the optimization of the precoder $\mathbf{W}$, which can be decomposed into a sequence of convex problems by employing our proposed distance majorization algorithm. Then, in Section IV, we consider the signal-dependent

(endogenous) interference due to the clutter generated by the scatterers proximity to the radar for designing the precoder $\mathbf{W}$, which is nonconvex since the objective function and the per-antenna power constraint are both nonconvex. We jointly exploit the distance majorization algorithm and fractional programming [47] to design an iterative algorithm for transforming the nonconvex optimization problem into a sequence of convex unconstrained problems.

III. SIGNAL-INDEPENDENT INTERFERENCE CASE

In this section, we first consider the signal-independent interference which is distributed as $\mathcal{CN}\left(\mathbf{0}, \mathbf{I}\right)$ [36]. The corresponding covariance matrix $\mathbf{R}_c$ is constant, i.e., $\mathbf{R}_c \triangleq \sum_{i=1}^{N}|\beta_i|^2\mathbf{a}_r(\psi_i)\mathbf{a}_t^T(\psi_i)$, where N is the number of clutters and β_i is the amplitude of the ith interfering signal located at angle ψ_i.

A. Distance Majorization Algorithm Induced Precoder Design

With no loss of optimality, by introducing additional phase shifting to $\mathbf{W}(:, i)$ for making $\mathcal{I}\left(\mathbf{h}_i^H\mathbf{W}(:, i)\right) = 0$, the SINR constraint (8b) can be recast as

$$\sqrt{1 + \frac{1}{R_i}}\mathbf{h}_i^H\mathbf{E}_i\mathbf{w} \geq ||\mathbf{H}_i\mathbf{w} + \mathbf{b}_i||_F, \ \mathcal{I}\left(\mathbf{h}_i^H\mathbf{E}_i\mathbf{w}\right) = 0, \quad (9)$$

where

$$\mathbf{w} = \left[\mathbf{W}^T(:, 1), \mathbf{W}^T(:, 2), \ldots, \mathbf{W}^T(:, K)\right]^T \in \mathbb{C}^{KN_t \times 1},$$

$$\mathbf{b}_i = \left[\mathbf{0}_{N_t}, \sigma_c^2\right]^T \in \mathbb{C}^{(K+1)\times 1},$$

$$\mathbf{E}_i = \left[\underbrace{\mathbf{0}, \ldots, \mathbf{0}}_{i-1}, \mathbf{I}, \underbrace{\mathbf{0}, \ldots, \mathbf{0}}_{K-i}\right] \in \mathbb{C}^{N_t \times KN_t},$$

$$\mathbf{H}_i = \begin{bmatrix}\mathrm{DIAG}\left(\mathbf{h}_i^H, \mathbf{h}_i^H, \ldots, \mathbf{h}_i^H\right) \\ \mathbf{0}_{N_t \times 1}^T\end{bmatrix} \in \mathbb{C}^{(K+1)\times N_t K}.$$

To facilitate the algorithm design, we use the following identity

$$\begin{bmatrix}\mathcal{R}(\mathbf{Hw}) \\ \mathcal{I}(\mathbf{Hw})\end{bmatrix} = \begin{bmatrix}\mathcal{R}(\mathbf{H}), & -\mathcal{I}(\mathbf{H}) \\ \mathcal{I}(\mathbf{H}), & \mathcal{R}(\mathbf{H})\end{bmatrix}\begin{bmatrix}\mathcal{R}(\mathbf{w}) \\ \mathcal{I}(\mathbf{w})\end{bmatrix}. \quad (10)$$

First, we reformulate the complex vector as its real counterpart, given by

$$\max_{\bar{\mathbf{w}}} \bar{\mathbf{w}}^T\bar{\mathbf{\Theta}}\bar{\mathbf{w}} \quad (11a)$$

$$\text{s.t.} \quad \sqrt{1 + \frac{1}{R_i}}\mathbf{g}_{i,1}\bar{\mathbf{w}} \geq ||\bar{\mathbf{H}}_i\bar{\mathbf{w}} + \bar{\mathbf{b}}_i||_F, \forall i \in \{1, \ldots, K\} \quad (11b)$$

$$\mathbf{g}_{i,2}\bar{\mathbf{w}} = 0, \ \forall i \in \{1, \ldots, K\} \quad (11c)$$

$$\mathrm{diag}\left(\mathbf{W}\mathbf{W}^H\right) = \frac{P_{\mathrm{tot}}}{N_t}\mathbf{I}, \quad (11d)$$

where

$$\bar{\mathbf{w}} = \left[\mathcal{R}(\mathbf{w})^T, \mathcal{I}(\mathbf{w})^T\right]^T, \mathbf{g}_{i,2} = \left[\mathcal{I}\left(\mathbf{h}_i^H\mathbf{E}_i\right), \mathcal{R}\left(\mathbf{h}_i^H\mathbf{E}_i\right)\right],$$

$$\bar{\mathbf{\Theta}} \triangleq \begin{bmatrix}\mathcal{R}\left(\mathbf{I}_K \otimes \mathbf{\Theta}\right), & -\mathcal{I}\left(\mathbf{I}_K \otimes \mathbf{\Theta}\right) \\ \mathcal{I}\left(\mathbf{I}_K \otimes \mathbf{\Theta}\right), & \mathcal{R}\left(\mathbf{I}_K \otimes \mathbf{\Theta}\right)\end{bmatrix}, \bar{\mathbf{b}}_i = \begin{bmatrix}\mathbf{b}_i \\ \mathbf{0}_{(N_t+1)\times 1}\end{bmatrix},$$

$$\bar{\mathbf{H}}_i = \begin{bmatrix}\mathcal{R}(\mathbf{H}_i), & -\mathcal{I}(\mathbf{H}_i) \\ \mathcal{I}(\mathbf{H}_i), & \mathcal{R}(\mathbf{H}_i)\end{bmatrix}, \ \mathbf{g}_{i,1} = \left[\mathcal{R}\left(\mathbf{h}_i^H\mathbf{E}_i\right), -\mathcal{I}\left(\mathbf{h}_i^H\mathbf{E}_i\right)\right].$$

Note that constraint (11c) is imposed for ensuring that the imaginary part $\mathcal{I}\left(\mathbf{h}_i^H \mathbf{E}_i \mathbf{w}\right) = 0$.

The challenges in handling problem (11) lie in the non-convexity of the objective function and constraint (11d). The nonconvexity can be handled by exploiting the strong duality of the nonconvex quadratic problem [51, Section 5.2.3]. In particular, through introducing a quadratic constraint, we have

$$\max_{\bar{\mathbf{w}}} \bar{\mathbf{w}}^T \bar{\mathbf{\Theta}} \bar{\mathbf{w}} \tag{12a}$$

$$\text{s.t.} (11b), (11c), (11d), \tag{12b}$$

$$\bar{\mathbf{w}}^T \bar{\mathbf{w}} \leq P_{\text{tot}}, \tag{12c}$$

where the added constraint (12c) does not shrink the feasible set due to per-antenna constraint (11d). Then, problem (11) and problem (12) have the same optimal solution.

By employing the penalty method [52], the inequality constraint (11b), constraint (11c), and per-antenna power constraint (11d) can be incorporated into the objective function with an appropriate penalty parameter ρ, i.e.,

$$\min_{\bar{\mathbf{w}}} -\bar{\mathbf{w}}^T \bar{\mathbf{\Theta}} \bar{\mathbf{w}} + \frac{\rho}{2} \sum_{1 \leq i \leq K} \text{dist}\left(\left[\mathbf{g}_{i,1}\bar{\mathbf{w}}; \bar{\mathbf{H}}_i \bar{\mathbf{w}} + \bar{\mathbf{b}}_i\right], \Omega_i\right)^2$$
$$+ \frac{\rho}{2} \text{dist}\left(\bar{\mathbf{w}}, \Xi\right)^2 + \frac{\rho}{2} \sum_i |\mathbf{g}_{i,2}\bar{\mathbf{w}}|^2, \tag{13a}$$

$$\text{s.t.} (12c), \tag{13b}$$

where $\Omega_i \triangleq \left\{\bar{\mathbf{w}} \mid \sqrt{1+\frac{1}{R_i}} \mathbf{g}_{i,1}\bar{\mathbf{w}} \geq \|\bar{\mathbf{H}}_i\bar{\mathbf{w}} + \bar{\mathbf{b}}_i\|_2\right\}$ and $\Xi \triangleq \left\{\mathbf{W} \mid \text{diag}\left(\mathbf{W}\mathbf{W}^H\right) = \frac{P_{\text{tot}}}{N_t}\mathbf{I}\right\}$.

Lemma 1: When problem (12) is feasible, as $\rho \to +\infty$, solving problem (13) yields the optimal solution of problem (12).

Proof: The proof is similar to the proof of [53, Theorem 17.1], which is omitted for brevity. ∎

However, the calculation of the distance $\text{dist}\left(\left[\mathbf{g}_{i,1}\bar{\mathbf{w}}; \bar{\mathbf{H}}_i\bar{\mathbf{w}} + \bar{\mathbf{b}}_i\right], \Omega_i\right)^2 = \inf_{\mathbf{y} \in \Omega} \|\left[\mathbf{g}_{i,1}\bar{\mathbf{w}}; \bar{\mathbf{H}}_i\bar{\mathbf{w}} + \bar{\mathbf{b}}_i\right] - \left[\mathbf{g}_{i,1}\mathbf{y}; \bar{\mathbf{H}}_i\mathbf{y} + \bar{\mathbf{b}}_i\right]\|_2^2$ and $\text{dist}\left(\bar{\mathbf{w}}, \Xi\right)^2$ are both complicated optimization problems. Therefore, it is challenging to solve problem (13) directly. As an alternative, we employ the majorization-minimization algorithm [54] to approximate the objective function of problem (13) as a sequence of tractable functions, as follows

$$\Phi\left(\bar{\mathbf{w}}\right) \triangleq \frac{\rho}{2} \sum_{1 \leq i \leq K} \left\|\left[\mathbf{g}_{i,1}\bar{\mathbf{w}}; \bar{\mathbf{H}}_i\bar{\mathbf{w}} + \bar{\mathbf{b}}_i\right] - \left[\hat{r}_i(k); \hat{\mathbf{f}}_i(k)\right]\right\|_2^2$$
$$- \bar{\mathbf{w}}^T \bar{\mathbf{\Theta}} \bar{\mathbf{w}} + \frac{\rho}{2} \|\bar{\mathbf{w}} - \hat{\mathbf{w}}(k)\|^2 + \frac{\rho}{2} \sum_{1 \leq i \leq K} |\mathbf{g}_{i,2}\bar{\mathbf{w}}|^2, \tag{14}$$

where $\left[\hat{r}_i(k); \hat{\mathbf{f}}_i(k)\right]$ is the vector $\left[\mathbf{g}_{i,1}\bar{\mathbf{w}}; \bar{\mathbf{H}}_i\bar{\mathbf{w}} + \bar{\mathbf{b}}_i\right]$ projected onto Ω, and $\hat{\mathbf{w}}(k)$ is the solution projected onto Ξ at the kth iteration.

Using (14), the convex approximation of problem (13) at the kth iteration is given by

$$\underset{\bar{\mathbf{w}}}{\text{minimize}} \, \Phi\left(\bar{\mathbf{w}}\right), \tag{15a}$$

$$\text{s.t.} \, \bar{\mathbf{w}}^T \bar{\mathbf{w}} \leq P_{\text{tot}}. \tag{15b}$$

Although problem (15) is the solution of a nonconvex optimization problem due to $-\bar{\mathbf{w}}^T \bar{\mathbf{\Theta}} \bar{\mathbf{w}}$, its optimal solution still satisfies its KKT condition due to the nonconvex quadratic problem with strong duality [51, Section 5.2.3]. The corresponding KKT condition is given as follows

$$-2\bar{\mathbf{\Theta}}\bar{\mathbf{w}} + \vartheta\bar{\mathbf{w}} + \rho\left(\bar{\mathbf{w}} - \hat{\mathbf{w}}\right) + \rho\mathbf{g}_{i,2}^T\mathbf{g}_{i,2}\bar{\mathbf{w}} +$$
$$\rho\left[\mathbf{g}_{i,1}, \bar{\mathbf{H}}_i\right]^T \left(\left[\mathbf{g}_{i,1}\bar{\mathbf{w}}; \bar{\mathbf{H}}_i\bar{\mathbf{w}} + \bar{\mathbf{b}}_i\right] - \left[\hat{r}_i(k); \hat{\mathbf{f}}(k)\right]\right) = 0, \tag{16}$$

$$\bar{\mathbf{w}}^H\bar{\mathbf{w}} \leq P_{\text{tot}}, \tag{17}$$

$$\vartheta \geq 0, \tag{18}$$

$$\vartheta\left(\bar{\mathbf{w}}^T\bar{\mathbf{w}} - P_{\text{tot}}\right) = 0, \tag{19}$$

where the multiplier ϑ is introduced for constraint (15b).

From the KKT condition above, we have

$$\left(-2\bar{\mathbf{\Theta}} + \vartheta\mathbf{I}_{2KN_t}\right)\bar{\mathbf{w}} + \sum_i \rho\mathbf{g}_{i,1}^T\left(\mathbf{g}_{i,1}\bar{\mathbf{w}} - \hat{r}_i(k)\right) +$$
$$\rho\left(\bar{\mathbf{w}} - \hat{\mathbf{w}}(k)\right) + \sum_i \bar{\mathbf{H}}_i^T\rho\left(\bar{\mathbf{H}}_i\bar{\mathbf{w}} + \bar{\mathbf{b}}_i - \hat{\mathbf{f}}_i(k)\right) +$$
$$\rho\sum_i \mathbf{g}_{i,2}^T\mathbf{g}_{i,2}\bar{\mathbf{w}} = \mathbf{0}.$$

Accordingly, the optimized $\bar{\mathbf{w}}$ can be obtained as

$$\bar{\mathbf{w}} = \mathbf{M}^{-1}\mathbf{N}, \tag{20}$$

where $\mathbf{M} \triangleq 2\rho^{-1}\bar{\mathbf{\Theta}} + \left(\rho^{-1}\vartheta^* + 1\right)\mathbf{I}_{2KN_t} + \sum_i \mathbf{g}_{i,2}^T\mathbf{g}_{i,2} + \sum_i \mathbf{g}_{i,1}^T\mathbf{g}_{i,1} + \sum_i \bar{\mathbf{H}}_i^T\bar{\mathbf{H}}_i$ and $\mathbf{N} \triangleq \hat{\mathbf{w}}(k) + \sum_i \mathbf{g}_{i,1}\hat{r}_i(k) - \sum_i \bar{\mathbf{H}}_i^T\left(\bar{\mathbf{b}}_i - \hat{\mathbf{f}}_i(k)\right)$. Besides, since $\bar{\mathbf{w}}$ is a decreasing function of ϑ^*, we can employ the bisection search algorithm [51] to find ϑ^* that satisfies (15b). Then, with the convergence of majorization-minimization algorithm [54, Section II-C], a KKT solution of problem (13) can be obtained by solving problem (15) iteratively.

From (20), it is obvious that the analytical solution of $\bar{\mathbf{w}}$ can be obtained with the projected solutions $\hat{r}_i(k)$ and $\hat{\mathbf{f}}_i(k)$ whose analytical solutions are given as follows.

Theorem 1: Denoting $r_i \triangleq \mathbf{g}_{i,1}\bar{\mathbf{w}}$, and $\mathbf{f}_i \triangleq \bar{\mathbf{H}}_i\bar{\mathbf{w}} + \bar{\mathbf{b}}_i$, the analytical result of $\left(\hat{r}_i(k), \hat{\mathbf{f}}_i(k)\right)$ projected onto Ω_i is given by (21) at the top of the next page, where $\alpha_i = \sqrt{1 + 1/R_i}$.

Proof: The proof is given in Appendix A. ∎

The penalty parameter ρ is imposed to achieve the tradeoff between satisfying the constraints and maximizing the sensing SINR. A large penalty parameter ρ tends more to obtain a feasible solution while a small ρ tends to maximize the sensing SINR. Hence, we exploit the widely adopted updating approach for designing ρ [55], [56]. In particular, we initialize $\rho = 1$ which results in a large sensing SINR that may violate the constraints in problem (11). Then, we gradually increase ρ to pull the solution towards the optimal solution in the feasible region.

To speed up the convergence rate, we incorporate Nesterov's acceleration strategy [52] into our proposed distance majorization algorithm which is summarized in Algorithm 1. In the following theorem, we will show the convergence of Algorithm 1 to a KKT solution of problem (12).

Theorem 2: Define that $c_{1,i}\left(\bar{\mathbf{w}}\right) \triangleq \text{dist}\left(\left[\mathbf{g}_{i,1}\bar{\mathbf{w}}; \bar{\mathbf{H}}_i\bar{\mathbf{w}} + \bar{\mathbf{b}}_i\right], \Omega_i\right)$, $c_2\left(\bar{\mathbf{w}}\right) \triangleq \text{dist}\left(\bar{\mathbf{w}}, \Xi\right)$,

$$\left(\hat{r}_i(k), \hat{\mathbf{f}}_i(k)\right) = \begin{cases} \left(\dfrac{[\|\mathbf{f}_i\|_2 + \alpha_i r_i]^+}{\alpha_i + \frac{1}{\alpha_i}}, \dfrac{[\|\mathbf{f}_i\|_2 + 1/\alpha_i r_i]^+}{\|\mathbf{f}_i\|_2 + 1/\alpha_i^2\|\mathbf{f}_i\|_2}\mathbf{f}_i\right), & \text{if } \alpha_i r_i < \|\mathbf{f}_i\|_2 \\ \left(r_i, \mathbf{f}_i\right), & \text{if } \alpha_i r_i \geq \|\mathbf{f}_i\|_2 \end{cases} \tag{21}$$

Algorithm 1 Proposed Distance Majorization Algorithm for Solving Problem (11)

1: Initialize $\rho = 1$, $c = 2$, $\rho_{\max} = 10^9$, $\bar{\mathbf{w}}(1) = \bar{\mathbf{w}}(0) \in \mathbb{R}^{2N_t K \times 1}$, the convergence tolerance $\epsilon = 10^{-4}$, $T = 30$, and $k = 1$.
2: **Repeat**
3: $\mathbf{z}(k) = \mathbf{w}(k) + \frac{k-1}{k+2}(\mathbf{w}(k) - \mathbf{w}(k-1))$,
4: Obtain $\left(\hat{r}_i(k), \hat{\mathbf{f}}_i(k)\right)$ with Theorem 1, and obtain $\hat{\mathbf{y}}(k) = \sqrt{\frac{P_{\text{tot}}}{N_t}}\bar{\mathbf{y}}./|\bar{\mathbf{y}}|$ by projecting $\bar{\mathbf{y}}$ into $\boldsymbol{\Xi}$
5: Obtain $\bar{\mathbf{w}}$ with (20),
6: Update $\rho = \min(\rho_{\max}, c\rho)$, every T iterations
7: $k = k + 1$,
8: **Until** $\|\mathbf{w}(k+1) - \mathbf{w}(k)\|_2 \leq \epsilon$.

---

and $c_{3,i}(\bar{\mathbf{w}}) \triangleq |\mathbf{g}_{i,2}\bar{\mathbf{w}}|$, $1 \leq i \leq K$. Suppose that a limit point $\bar{\mathbf{w}}^*$ obtained by Algorithm 1 makes $\Upsilon(\bar{\mathbf{w}}^*, \lambda) \triangleq -2\bar{\boldsymbol{\Theta}}\bar{\mathbf{w}}^* + 2\lambda\bar{\mathbf{w}}^* + \sum_{1 \leq i \leq K} \rho c_{1,i}(\bar{\mathbf{w}}^*) \nabla_{\bar{\mathbf{w}}^*} c_{1,i}(\bar{\mathbf{w}}^*) + \sum_{1 \leq i \leq K} \rho c_{3,i}(\bar{\mathbf{w}}^*) \nabla_{\bar{\mathbf{w}}^*} c_{3,i}(\bar{\mathbf{w}}^*) + \rho c_2(\bar{\mathbf{w}}^*) \nabla_{\bar{\mathbf{w}}^*} c_2(\bar{\mathbf{w}}^*) \to \mathbf{0}$ as $\rho \to +\infty$, where λ is Lagrange multiplier associated with constraint (12c). Then, if $\bar{\mathbf{w}}^*$ is feasible and the gradients $\nabla_{\bar{\mathbf{w}}^*} c_{1,i}(\bar{\mathbf{w}}^*)$, $\nabla_{\bar{\mathbf{w}}^*} c_2(\bar{\mathbf{w}}^*)$, and $\nabla_{\bar{\mathbf{w}}^*} c_{3,i}(\bar{\mathbf{w}}^*)$ are all linearly independent, $\bar{\mathbf{w}}^*$ is a KKT solution of problem (12).

Proof: The proof is given in Appendix B. ∎

Remark 1: As verified by [42, Section 4], the convergence of distance-majoriation algorithm still holds for the general nonconvex optimization due to Zangwill's global convergence theorem.

B. Computational Complexity Analysis

The computational complexity of our proposed Algorithm 1 is dominated by (20). In particular, $\rho^{-1}\bar{\boldsymbol{\Theta}} + \sum_{1 \leq i \leq K} \mathbf{g}_{i,2}^T \mathbf{g}_{i,2} + \sum_{1 \leq i \leq K} \mathbf{g}_{i,1}^T \mathbf{g}_{i,1} + \sum_{1 \leq i \leq K} \bar{\mathbf{H}}_i^T \bar{\mathbf{H}}_i = \begin{bmatrix} \mathbf{A}, & \mathbf{B} \\ \mathbf{C}, & \mathbf{A} \end{bmatrix}$ where $\mathbf{A}$, $\mathbf{B}$, and $\mathbf{C}$ are all block diagonal matrices. Specifically, $\mathbf{A} = \text{DIAG}(\mathbf{A}_1, \mathbf{A}_2, \ldots, \mathbf{A}_K)$, $\mathbf{B} = \text{DIAG}(\mathbf{B}_1, \mathbf{B}_2, \ldots, \mathbf{B}_K)$, $\mathbf{C} = \text{DIAG}(\mathbf{C}_1, \mathbf{C}_2, \ldots, \mathbf{C}_K)$,

$$\mathbf{A}_i \triangleq \sum_{1 \leq k \leq K} \left(\mathcal{R}\left(\mathbf{h}_k^H\right)^T \mathcal{R}\left(\mathbf{h}_k^H\right) + \mathcal{I}\left(\mathbf{h}_k^H\right)^T \mathcal{I}\left(\mathbf{h}_k^H\right)\right)$$
$$+ \mathcal{R}\left(\mathbf{h}_i^H\right)^T \mathcal{R}\left(\mathbf{h}_i^H\right) + \left(\rho^{-1}(\vartheta^* + \varrho) + 1\right)\mathbf{I}_{N_t}$$
$$+ \mathcal{I}\left(\mathbf{h}_i^H\right)^T \mathcal{I}\left(\mathbf{h}_i^H\right) + \rho^{-1}\mathcal{R}(\boldsymbol{\Theta}),$$

$$\mathbf{B}_i \triangleq \sum_{1 \leq k \leq K} \left(-\mathcal{R}\left(\mathbf{h}_k^H\right)^T \mathcal{I}\left(\mathbf{h}_k^H\right) + \mathcal{I}\left(\mathbf{h}_k^H\right)^T \mathcal{R}\left(\mathbf{h}_k^H\right)\right)$$
$$- \mathcal{R}\left(\mathbf{h}_i^H\right)^T \mathcal{I}\left(\mathbf{h}_i^H\right) - \mathcal{I}\left(\mathbf{h}_i^H\right)^T \mathcal{R}\left(\mathbf{h}_i^H\right) - \rho^{-1}\mathcal{I}(\boldsymbol{\Theta}),$$

$$\mathbf{C}_i \triangleq \sum_{1 \leq k \leq K} \left(-\mathcal{I}\left(\mathbf{h}_k^H\right)^T \mathcal{R}\left(\mathbf{h}_k^H\right) + \mathcal{R}\left(\mathbf{h}_k^H\right)^T \mathcal{I}\left(\mathbf{h}_k^H\right)\right)$$
$$- \mathcal{I}\left(\mathbf{h}_i^H\right)^T \mathcal{R}\left(\mathbf{h}_i^H\right) - \mathcal{I}\left(\mathbf{h}_i^H\right)^T \mathcal{R}\left(\mathbf{h}_i^H\right) + \rho^{-1}\mathcal{I}(\boldsymbol{\Theta}),$$

Then, with [57, eq. (1.7.12)], the inverse matrix $\mathbf{M}^{-1}$ is

$$\begin{bmatrix} \left(\mathbf{A} - \mathbf{B}\mathbf{A}^{-1}\mathbf{C}\right)^{-1}, & -\left(\mathbf{A} - \mathbf{B}\mathbf{A}^{-1}\mathbf{C}\right)^{-1}\mathbf{B}\mathbf{A}^{-1} \\ -\left(\mathbf{A} - \mathbf{C}\mathbf{A}^{-1}\mathbf{B}\right)^{-1}\mathbf{C}\mathbf{A}^{-1}, & \left(\mathbf{A} - \mathbf{C}\mathbf{A}^{-1}\mathbf{B}\right)^{-1} \end{bmatrix},$$

and the complexity of calculating $\bar{\mathbf{w}}$ in (20) is $\mathcal{O}\left(KN_t^{2.373}\right)$ when we employ the Coppersmith-Winograd algorithm to calculate the matrix inversion. Denoting by I_{DM} the number of iterations in our proposed distance majorization algorithm, the corresponding complexity is $\mathcal{O}\left(\mathrm{I}_{\text{DM}} K N_t^{2.373}\right)$.

In comparison, the worst-case computational complexity of the considered benchmark algorithm given in Appendix C is determined by solving an SDP problem. From [58], we know that the worst-case complexity of solving an SDP problem is $\mathcal{O}\left(n_{\text{sdp}}^{1/2}\left(m_{\text{sdp}}n_{\text{sdp}}^3 + m_{\text{sdp}}^2 n_{\text{sdp}}^2 + m_{\text{sdp}}^3\right)\right)\log(1/\epsilon_{\text{sdp}})$, where m_{sdp} is the number of semidefinite cone constraints, n_{sdp} is the dimension of the semidefinite cone, and ϵ_{sdp} is the solution accuracy. Then, after inspecting problem (61), the worst-case computational complexity of the benchmark algorithm is $\mathcal{O}\left(\mathrm{I}_{\text{sdp}}\left(KN_t^7 + K^2 N_t^5\right)\log(1/\epsilon_{\text{sdp}})\right)$, where I_{sdp} is the number of iterations.

Compared with the SDP-based benchmark algorithm, our proposed distance majorization induced algorithm has much lower computation complexity.

IV. SIGNAL-DEPENDENT CLUTTER CASE

Different from the previous section, we consider K signal-dependent clutters in this section. In particular, the corresponding received signal is given by

$$\mathbf{y}_0 = \mathbf{A}(\upsilon)\mathbf{W}\mathbf{s} + \sum_{i=1}^K \beta_i \mathbf{B}(\psi_i)\mathbf{W}\mathbf{s} + \mathbf{z}_0, \tag{22}$$

where $\mathbf{B}(\psi_i) \triangleq \boldsymbol{\alpha}_r(\psi_i)\boldsymbol{\alpha}_t^T(\psi_i)$.

Following the signal-independent clutter case, the optimal radar output SINR for K signal-dependent clutters can be derived as

$$\hat{\rho}(\mathbf{W}) = \text{Tr}\left(\mathbf{s}^H \mathbf{W}^H \mathbf{A}^H(\upsilon)\left(\hat{\mathbf{R}}_c + \mathbf{z}_0 \mathbf{z}_0^H\right)^{-1}\mathbf{A}(\upsilon)\mathbf{W}\mathbf{s}\right)$$
$$= \text{Tr}\left(\frac{\mathbf{s}\mathbf{s}^H}{L}\mathbf{W}^H \mathbf{A}^H(\upsilon)\left(\frac{\hat{\mathbf{R}}_c}{L} + \frac{\mathbf{z}_0 \mathbf{z}_0^H}{L}\right)^{-1}\mathbf{A}(\upsilon)\mathbf{W}\right)$$
$$\approx \text{Tr}\left(\hat{\boldsymbol{\Theta}}\mathbf{W}\mathbf{W}^H\right), \tag{23}$$

where $\hat{\mathbf{R}}_c = \sum_{i=1}^K \beta_i^2 \mathbf{B}(\psi_i)\mathbf{W}\mathbf{s}\mathbf{s}^H \mathbf{W}^H \mathbf{B}^H(\psi_i)$ and $\hat{\boldsymbol{\Theta}} \triangleq \mathbf{A}^H(\upsilon)\left(\sum_{i=1}^K \beta_i^2 \mathbf{B}(\psi_i)\mathbf{W}\mathbf{W}^H \mathbf{B}^H(\psi_i) + \mathbf{I}_K\right)^{-1}\mathbf{A}(\upsilon)$.

Through introducing auxiliary variables $r_i, v_i, \mathbf{f}_i$, and $\mathbf{Y}$, the precoder design for maximizing the radar output SINR in the

presence of signal-dependent interference can be built as

$$\underset{\mathbf{W}}{\text{maximize}}\ \hat{\rho}\left(\mathbf{W}\right) \tag{24a}$$

$$\text{s.t.}\ \sqrt{1+\frac{1}{R_i}}r_i \geq ||\mathbf{f}_i||_F, \tag{24b}$$

$$r_i = \mathbf{g}_{i,1}\bar{\mathbf{w}},\ \mathbf{f}_i = \bar{\mathbf{H}}_i\bar{\mathbf{w}} + \bar{\mathbf{b}}_i,\ \bar{\mathbf{w}} = \bar{\mathbf{y}}, \tag{24c}$$

$$v_i = \mathbf{g}_{i,2}\bar{\mathbf{w}},\ v_i = 0, \tag{24d}$$

$$\text{diag}\left(\mathbf{Y}\mathbf{Y}^H\right) = \frac{P_{\text{tot}}}{N_t}\mathbf{I}. \tag{24e}$$

Problem (24) is challenging to solve directly, since the objective function and constraint (24e) are both nonconvex. To complicate matters further, even if we adopt the SDR approach given in Appendix C, the objective function is still nonconvex and a feasible solution of problem (24) is still difficult to obtain by solving its SDR-relaxed version.

To handle the nonconvexity of the objective function, we employ fractional programming [47, Theorem 1] to obtain an equivalent formulation of $\hat{\rho}\left(\mathbf{W}\right)$, given by

$$\hat{\rho}\left(\mathbf{W}\right) = \underset{\mathbf{\Gamma}}{\text{maximize}}\ \mathbf{\Xi}\left(\mathbf{W}, \mathbf{\Gamma}\right), \tag{25}$$

where $\mathbf{\Xi}\left(\mathbf{W}, \mathbf{\Gamma}\right)$ is given by (27) at the top of the next page and the optimal $\mathbf{\Gamma}^*$ is given by [47, Theorem 1]

$$\mathbf{\Gamma}^* = \left(\sum_{i=1}^{K}\beta_i^2\mathbf{B}(\psi_i)\mathbf{W}\mathbf{W}^H\mathbf{B}^H(\psi_i) + \mathbf{I}_K\right)^{-1}\mathbf{A}(v)\mathbf{W}. \tag{26}$$

In the following, we employ (25) to design an alternating algorithm for obtaining an efficient solution of problem (24).

In particular, we first employ the matrix vectorization operation [57, Section 1.11.2] to obtain its vector formulation given by (29) at the top of the next page. Moreover, to facilitate the optimization algorithm design, we employ (10) to reformulate (29) in the following real-valued form

$$\tilde{\mathbf{\Xi}}\left(\bar{\mathbf{w}}, \mathbf{\Gamma}\right) = 2\bar{\mathbf{w}}^T\mathbf{\Omega}_0 - \bar{\mathbf{w}}^T\mathbf{\Omega}_1\bar{\mathbf{w}} - \text{Tr}\left(\mathbf{\Gamma}^H\mathbf{\Gamma}\right), \tag{28}$$

where

$$\mathbf{\Omega}_0 \triangleq \begin{bmatrix} \mathcal{R}\left(\text{vec}\left(\mathbf{A}^H(v)\mathbf{\Gamma}\right)\right) \\ \mathcal{I}\left(\text{vec}\left(\mathbf{A}^H(v)\mathbf{\Gamma}\right)\right) \end{bmatrix},$$

$$\mathbf{\Omega}_1 \triangleq \begin{bmatrix} \mathcal{R}\left(\mathbf{\Lambda}\right), & -\mathcal{I}\left(\mathbf{\Lambda}\right) \\ \mathcal{I}\left(\mathbf{\Lambda}\right), & \mathcal{R}\left(\mathbf{\Lambda}\right) \end{bmatrix},$$

$$\mathbf{\Lambda} \triangleq \sum_{i=1}^{K}\alpha_i^2\left(\mathbf{I}_K\otimes\left(\mathbf{A}^H(\theta_i)\mathbf{\Gamma}\mathbf{\Gamma}^H\mathbf{A}(\theta_i)\right)\right).$$

Therefore, considering the signal-dependent clutter case, with the fixed $\mathbf{\Gamma}$, the precoder optimization for maximizing the radar sensing SINR under the communications QoS requirements and per-antenna power constraint can be formulated as

$$\underset{\mathbf{W}}{\text{maximize}}\ \tilde{\mathbf{\Xi}}\left(\bar{\mathbf{w}}, \mathbf{\Gamma}\right)$$
$$\text{s.t.}\ (24b), (24c), (24d), (24e). \tag{30}$$

Then, following the distance majorization algorithm described in Section III, the optimized $\mathbf{W}$ can be obtained by solving a

---

Algorithm 2 Proposed Distance Majorization Algorithm for Handling Problem (30)

1: Initialize $\rho = 1$, $c = 2$, $\rho_{\max} = 10^9$, $\bar{\mathbf{w}}(1) = \bar{\mathbf{w}}(0) \in \mathbb{R}^{2N_tK\times 1}$, the convergence tolerance $\epsilon = 10^{-4}$, $T = 30$, and $k = 1$.
2: **Repeat**
3: $\mathbf{z}(k) = \mathbf{w}(k) + \frac{k-1}{k+2}\left(\mathbf{w}(k) - \mathbf{w}(k-1)\right)$,
4: Obtain $\left(\hat{r}_i(k), \hat{\mathbf{f}}_i(k)\right)$ with Theorem 1,
5: Obtain $\tilde{\mathbf{w}}$ with (20),
6: Update $\rho = \min\left(\rho_{\max}, c\rho\right)$, every T iterations
7: $k = k + 1$,
8: **Until** $||\mathbf{w}(k+1) - \mathbf{w}(k)||_2 \leq \epsilon$.

Algorithm 3 Proposed Alternating Optimization Algorithm for Handling Problem (24)

1: Initialize $\mathbf{\Gamma}^* \in \mathbb{C}^{N_t\times K}$, the maximum number of iterations $\mathbf{I}_{\max}$, and $n = 1$.
2: **Repeat**
3: Obtaining $\bar{\mathbf{w}}^*$ by solving problem (30) with Algorithm 2,
4: Obtaining $\mathbf{\Gamma}^*$ with (26),
5: $n = n + 1$,
6: **Until** $\frac{|\tilde{\mathbf{\Xi}}(\bar{\mathbf{w}}(n+1), \mathbf{\Gamma}(n+1)) - \tilde{\mathbf{\Xi}}(\bar{\mathbf{w}}(n), \mathbf{\Gamma}(n))|}{\tilde{\mathbf{\Xi}}(\bar{\mathbf{w}}(n), \mathbf{\Gamma}(n))} \leq \epsilon$, or the maximum number of iterations $\mathbf{I}_{\max}$ is satisfied.

---

sequence of penalized problems, given by

$$\underset{\bar{\mathbf{w}}, \bar{\mathbf{y}}, v_i, r_i, \mathbf{f}_i}{\text{maximize}}\ \tilde{\mathbf{\Xi}}\left(\bar{\mathbf{w}}, \mathbf{\Gamma}\right) + \frac{\rho}{2}||\bar{\mathbf{y}} - \hat{\mathbf{y}}(k)||^2 + \frac{\rho}{2}\sum_i|v_i|^2 +$$

$$\frac{\rho}{2}\sum_{1\leq i\leq K}\left|\left|\left[r_i, \mathbf{f}_i^T\right]^T - \left[\hat{r}_i(k), \hat{\mathbf{f}}_i^T(k)\right]^T\right|\right|_2^2$$

$$\text{s.t.}\ (24c),\ (24d). \tag{31}$$

It is worth noting that different from problem (13), problem (31) is convex whose optimal solution satisfies its KKT condition given by

$$2\mathbf{\Omega}_0 - 2\mathbf{\Omega}_1\bar{\mathbf{w}} - \sum_{1\leq i\leq K}\hat{\theta}_i\mathbf{g}_{i,1}^T - \sum_{1\leq i\leq K}\bar{\mathbf{H}}_i^T\hat{\mathbf{\lambda}}_i + \hat{\mathbf{\eta}}$$

$$- \sum_{1\leq i\leq K}\hat{\tau}_i\mathbf{g}_{i,2}^T = \mathbf{0},$$

$$\hat{\theta}_i + \rho\left(r_i - \hat{r}_i(k)\right) = 0,$$

$$\hat{\mathbf{\lambda}}_i + \rho\left(\mathbf{f}_i - \hat{\mathbf{f}}_i(k)\right) = \mathbf{0},$$

$$-\hat{\mathbf{\eta}} + \rho\left(\bar{\mathbf{y}} - \hat{\mathbf{y}}(k)\right) = \mathbf{0},$$

$$\hat{\tau}_i + \rho v_i = 0.$$

From the KKT condition above, the optimized $\bar{\mathbf{w}}$ can be derived as

$$\bar{\mathbf{w}} = \hat{\mathbf{M}}^{-1}\hat{\mathbf{N}}, \tag{32}$$

where $\hat{\mathbf{M}} \triangleq \frac{2}{\rho}\mathbf{\Omega}_1 + \mathbf{I}_{2KN_t} + \sum_i\mathbf{g}_{i,2}^T\mathbf{g}_{i,2} + \sum_{1\leq i\leq K}\mathbf{g}_{i,1}^T\mathbf{g}_{i,1} + \sum_{1\leq i\leq K}\bar{\mathbf{H}}_i^T\bar{\mathbf{H}}_i$ and $\hat{\mathbf{N}} \triangleq \hat{\mathbf{y}}(k) + \frac{2}{\rho}\mathbf{\Omega}_0 + \sum_{1\leq i\leq K}\mathbf{g}_{i,1}\hat{r}_i(k) - \sum_{1\leq j\leq K}\bar{\mathbf{H}}_i^T\left(\bar{\mathbf{b}}_i - \hat{\mathbf{f}}_i(k)\right)$.

Finally, Algorithm 2 summarizes the proposed distance majorization algorithm for handling problem (30).

Therefore, with the alternating algorithm, an efficient solution of problem (24) can be obtained by updating $\mathbf{\Gamma}$ and $\mathbf{W}$ alternatively. Algorithm 3 summarizes the corresponding optimization algorithm.

Remark 2: The monotonic property of Algorithm 3 can be proved by following the inexact block coordinate descent algorithm studied in [59]. Specifically, considering the solution

$$\Xi\left(\mathbf{W},\boldsymbol{\Gamma}\right) \triangleq \mathrm{Tr}\left(2\mathcal{R}\left(\mathbf{W}^H\mathbf{A}^H(\upsilon)\boldsymbol{\Gamma}\right) - \boldsymbol{\Gamma}^H\left(\sum_{i=1}^{K}\alpha_i^2\mathbf{B}(\psi_i)\mathbf{W}\mathbf{W}^H\mathbf{B}^H(\psi_i) + \mathbf{I}_K\right)\boldsymbol{\Gamma}\right) \tag{27}$$

$$\hat{\tilde{\Xi}}\left(\mathbf{w},\boldsymbol{\Gamma}\right) \triangleq \mathbf{w}^H\mathrm{vec}\left(\mathbf{A}^H(\upsilon)\boldsymbol{\Gamma}\right) + \mathrm{vec}^H\left(\mathbf{A}^H(\upsilon)\boldsymbol{\Gamma}\right)\mathbf{w} - \mathbf{w}^H\left(\sum_{i=1}^{K}\alpha_i^2\left(\mathbf{I}_K\otimes\left(\mathbf{B}^H(\psi_i)\boldsymbol{\Gamma}\boldsymbol{\Gamma}^H\mathbf{B}(\psi_i)\right)\right)\right)\mathbf{w} - \mathrm{Tr}\left(\boldsymbol{\Gamma}^H\boldsymbol{\Gamma}\right) \tag{29}$$

$(\bar{\mathbf{w}}(n), \boldsymbol{\Gamma}(n))$ obtained at the nth iteration, since $\bar{\mathbf{w}}(n)$ is a feasible solution of problem (30) at the $(n+1)$th iteration, it is obvious that $\hat{\tilde{\Xi}}(\bar{\mathbf{w}}(n+1), \boldsymbol{\Gamma}(n)) \geq \hat{\tilde{\Xi}}(\bar{\mathbf{w}}(n), \boldsymbol{\Gamma}(n))$, where $\bar{\mathbf{w}}(n+1)$ is the solution obtained by Algorithm 3 at the $(n+1)$th iteration. Besides, considering (25), we have $\hat{\tilde{\Xi}}(\bar{\mathbf{w}}(n+1), \boldsymbol{\Gamma}(n+1)) \geq \hat{\tilde{\Xi}}(\bar{\mathbf{w}}(n+1), \boldsymbol{\Gamma}(n)) \geq \hat{\tilde{\Xi}}(\bar{\mathbf{w}}(n), \boldsymbol{\Gamma}(n))$. Therefore, in the iteration of Algorithm 3, the objective function $\Xi(\mathbf{W}, \boldsymbol{\Gamma})$ has been proved to be monotone increasing and its convergence can be guaranteed.

V. SIMULATION RESULTS

This section evaluates the performance of our proposed precoder design algorithm in the presence of signal-independent interference and signal-dependent clutter via computer simulations. Following [25], the noise powers are set as $\sigma_c^2 = \sigma_r^2 = 0$ dBm and the communication channel is assumed to be Rayleigh fading whose elements follow $\mathcal{CN}(0, 1)$. Besides, we assume that the reflecting coefficient of the target, $\alpha = \sqrt{0.5}$, and consider three fixed interfering signals with the spatial angles of $\psi_1 = 10^o$, $\psi_2 = -60^o$, $\psi_3 = 60^o$, and their amplitudes $|\beta_i|^2 = 0.1$, $i = 1, 2, 3$ [49]. For the performance comparison, the "SDR-based algorithm (SDRBA)" given in Appendix C is adopted as the benchmark, where problem (8) is first transformed into an SDP and the rank constraint is handled by the penalty algorithm.

A. Signal Independent Interference Case

In this subsection, we first consider the signal independent interference case, where $\mathbf{R}_c \triangleq \sum_{i=1}^{3}|\beta_i|^2\mathbf{a}_r(\psi_i)\mathbf{a}_t^T(\psi_i)$ and a target with the spatial angle of $\upsilon = 0^o$. In Fig. 2, the beampatterns optimized by the SDRBA and our proposed algorithm (PA) are both shown. Following [36], the beampattern is defined as $P(\theta) = |\mathbf{t}^H\mathbf{A}(\upsilon)\mathbf{w}|^2$ (dBm), where $\mathbf{t}$ is the receiver filter defined in (6). The two design approaches both place the main beam at the spatial angle of the target, and the nulling beamformer at the interfering signals' spatial angles $\psi_1 = 10^o$, $\psi_2 = -60^o$, $\psi_3 = 60^o$. Furthermore, it is clear that PA outperforms SDRBA, where the power gains of SDR and PA at υ are 41.28 dBm and 40.6 dBm, respectively, when $N_t = 20$ and $K = 10$, and the power gains are 36.85 dBm and 35.24 dBm, respectively, when $N_t = 10$ and $K = 8$. Besides, PA also achieves a lower nulling beamformer gain than SDR at the interference, which results in a larger SINR received at the radar receiver. On the other hand, by comparing the beampatterns with $N_t = 20$ and $N_t = 10$, we can find that the maximum peak to sidelobe ratio reduces with the decreasing
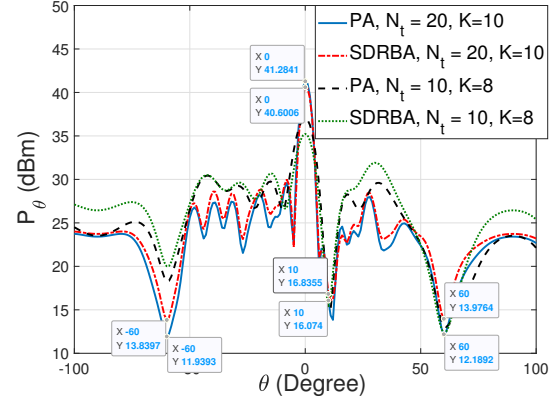

Fig. 2. The optimized beampatterns comparison for $N_t = 20$, $N_r = 10$, $K = 10$, $P_{\mathrm{tot}} = 20$ dBm, and $R_i = 5$ dB.
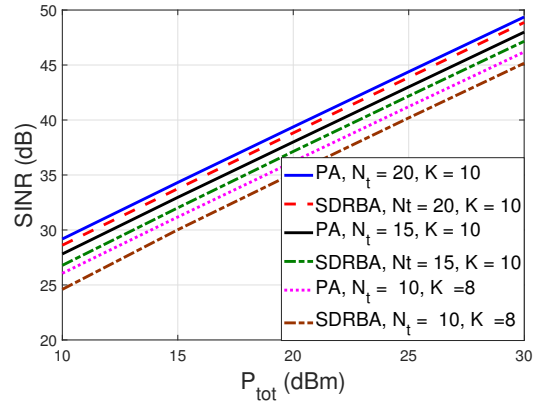

Fig. 3. The sensing SINR versus the total transmit power P_{tot} for $N_r = 10$, $R_i = 0$ dB, and different N_t and K.

N_t. Furthermore, the power gain at the direction of the target decreases with the decreasing N_t, and the corresponding width of the beam increases, since the decreasing N_t reduces the spatial DoF which results in a wider spatial beamformer and lower power gains at the desired direction.

Fig. 3 illustrates the behavior of the sensing SINR at the radar receiver achieved by SDRBA and PA versus the total transmit power, P_{tot}. With increasing P_{tot}, the sensing SINR increases, since more power budget can be utilized to sense the target and satisfy the SINR constraints of multiple users. Furthermore, the sensing SINR also increases with the increasing N_t. This is because increasing N_t can realize an improved beampattern with decreasing beamwidth that improves the
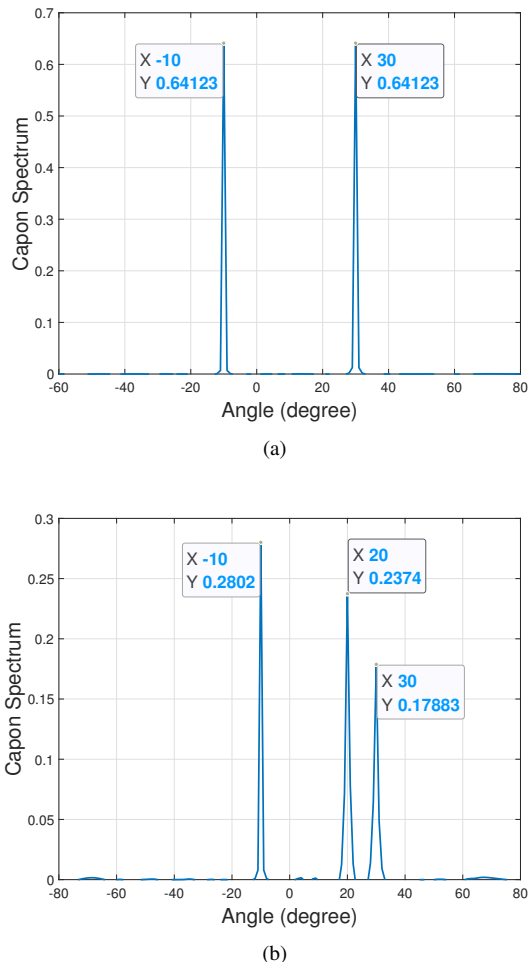
(a)

(b)

Fig. 4. Capon spatial spectral estimation in presence of signal-independent interference: (a) two targets with $v_1 = -10^o$ and $v_2 = 30^o$; (b) three targets with $v_1 = -10^o$, $v_2 = 20^o$, and $v_3 = 30^o$

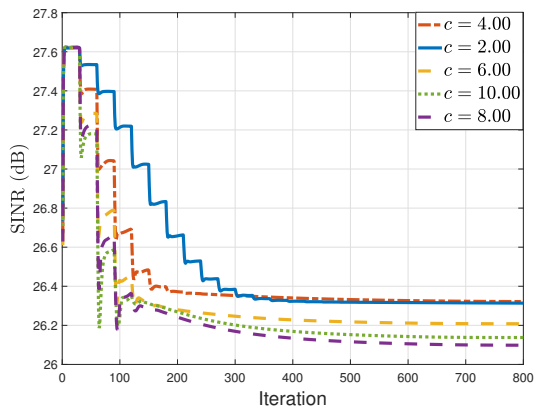Fig. 5. The convergence rate of proposed Algorithm 1 with $N_t = N_r = 10$, $K = 8$, $P_{tot} = 10$ dBm, $R_i = 3$ dB, and different penalty c.

energy concentration. Moreover, increasing N_t results in the increasing array gains that also increase the sensing SINR.

For measuring the radar sensing performance in the presence of signal-independent interference, we consider a scenario with multiple targets located at different spatial angles to

plot the Capon spatial spectrum in Fig. 4, which is calculated with the least squares Capon method given in [60, Section III-A]. From Fig. 4, we can find that the Capon spatial spectrum has narrow peaks only at the target angles, which confirms the angle estimation accuracy of the optimized beamforming.

Fig. 5 illustrates the impact of the penalty c on the convergence rate of our proposed Algorithm 1 for three targets locating at the spatial angles $v_1 = 0^o$, $v_2 = 20^o$, and $v_3 = 40^o$ with the reflection coefficients $\alpha_1 = \alpha_2 = \alpha_3 = \sqrt{0.5}$ [49]. From Fig. 5, we can find that a larger c would improve the convergence rate. But after increasing c beyond a threshold, the achievable performance would deteriorate. Therefore, c should be designed cautiously for achieving a tradeoff between the achievable performance and convergence rate.

In Fig. 6, we consider a single moving vehicle to show the impact of imperfect angle estimation on the sensing performance during the target tracking. Specifically, we consider the vehicle-to-infrastructure communication used in [61] and adopt the EKF to estimate the angles of a moving vehicle. For illustrating the impact of imperfect angle information on the sensing performance, we do not consider the change of the reflection coefficient. For completeness, the state evolution model of the target is given as follows [61]

$$\begin{cases} v_n = v_{n-1} + d_{n-1}^{-1} v_{n-1} \Delta T \sin\theta_{n-1} + \omega_v, \\ d_n = d_{n-1} - v_{n-1} \Delta T \cos\theta_{n-1} + \omega_d, \\ q_n = q_{n-1} + \omega_q, \end{cases} \quad (33)$$

where $\omega_v \sim \mathcal{CN}\left(0, \sigma_v^2\right)$, $\omega_d \sim \mathcal{CN}\left(0, \sigma_d^2\right)$, and $\omega_q \sim \mathcal{CN}\left(0, \sigma_q^2\right)$. In particular, following [61], we set the initial velocity $q_0 = 20$ m/s, the initial distance $d_0 = 25$ m, the initial angle $v_0 = 9^o$, $\sigma_v = 0.02^o$, $\sigma_\theta = 0.02^o$, $\sigma_d = 0.1$, and $\sigma_v^2 = 0.1$. Besides, the other system parameters are set as: measurement noise variance of 0.1, frequency of 30 GHz, total transmit power of $P_{tot} = 10$ dBm, and three interfering signals with spatial angles of $\psi_1 = -(v + 10^o)$, $\psi_2 = v + 20^o$, and $\psi_3 = v + 10^o$. Based on the state evolution model and observation model, EKF is employed to track the variation of the angle of the vehicle [61, Section III-A]. Fig. 6(a) and Fig. 6(b) respectively show the estimated angle tracking performance and sensing SINR for PA and SDRBA comparing with real ones. From the simulation results, we can find that when the EKF can track a moving target, the sensing performance of the proposed DFRC precoder design can meet the target. In particular, although the imperfect angle information predicted by EKF reduces the sensing SINR, the performance degradation is slight, which confirms the performance of our proposed DFRC precoder design approach in the target tracking.

B. Signal Dependent Clutter Case

In this subsection, we consider three targets and interfering signals due to clutter with the same parameters as the signal independent interference case, as described by (22). Our proposed Algorithm 3 adopts the alternating algorithm to handle the percoder optimization in the presence of clutters, i.e., problem (24) through optimizing $\mathbf{W}$ and $\mathbf{\Gamma}$ alternatively. Fig. 7 first shows the average convergence behavior of our
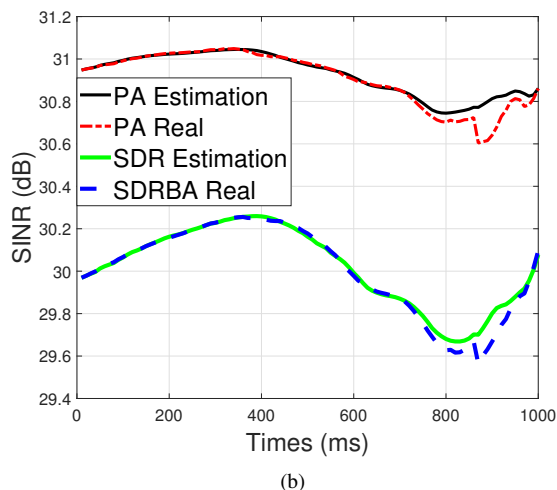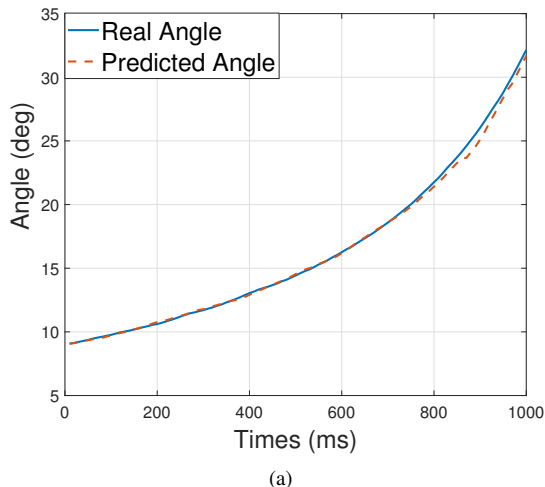
(a)

Fig. 7. Average convergence rate of our proposed Algorithm 3 with $N_r = 10$, $R_i = 3$ dB, $P_{\text{tot}} = 10$ dBm and different N_t and K.

(b)

Fig. 6. The sensing SINR for the radar tracking scenario with $N_t = 15$, $N_r = 20$, and $K = 10$ in the presence of signal-independent interference: (a) Angle tracking performances of EKF; (b) Sensing SINR comparison

Fig. 8. The optimized beampattern comparison for multiple targets with $N_r = 10$, $K = 10$, $P_{\text{tot}} = 20$ dBm, $R_i = 0$ dB, and different N_t

proposed Algorithm 3, whose results are obtained by averaging over 500 channel realizations. Algorithm 3 takes about 10 iterations to converge to a stable solution, which verifies the fast convergence rate and the efficiency of our proposed alternating algorithm. Moreover, changing the system parameters, e.g., the number of transmit antennas and served users does not have a significant effect on the convergence rate of Algorithm 3, which confirms its robustness.

Fig. 8 plots the optimized beampattern for different N_t, where we observe that the beampatterns all radiate the highest power at the target angles. However, the beamwidth at the spatial angle of the target increases with the decreasing N_t, since when the DoF is not sufficient, the beam should be widened to support multiuser broadcasting and radar sensing simultaneously.

Fig. 9 shows the optimized beampattern for different K. With the increasing K, more resources should be sacrificed to satisfy the SINR constraints of multiple users. Then, the corresponding resource used for radar sensing decreases accordingly. Therefore, from the simulation results in Fig.
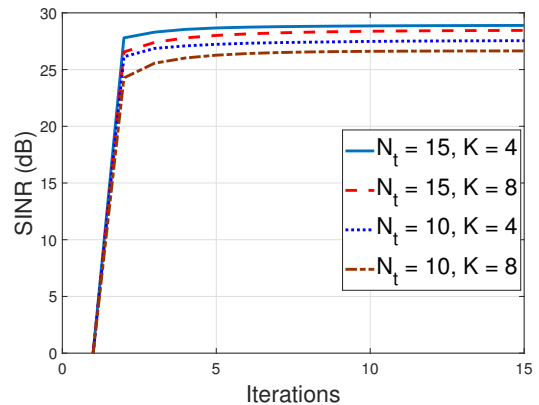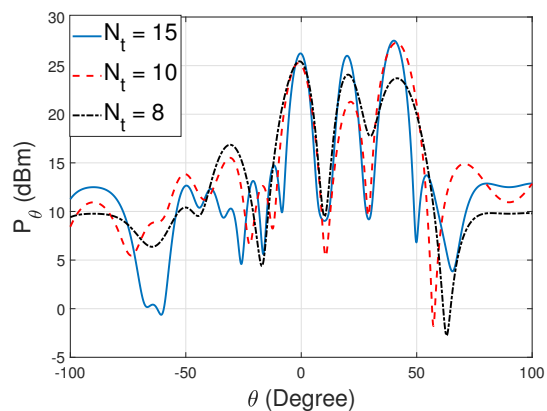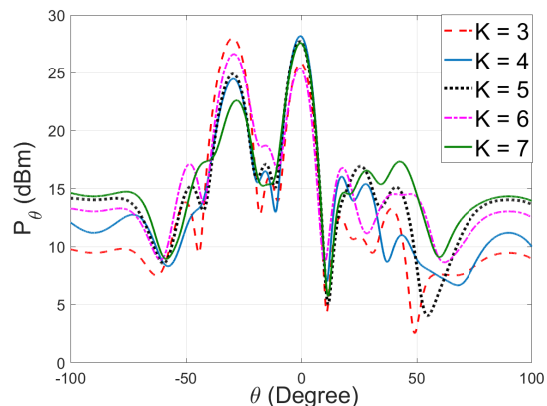

Fig. 9. The optimized beampattern comparison for multiple targets with $N_r = 10$, $N_t = 10$, $P_{\text{tot}} = 10$ dBm, $R_i = 5$ dB, and different K.

9, we can find that the power radiated at the target angle decreases and the corresponding beamwidth also increases. Moreover, the sidelobe also increases for serving multiple communication users. These simulation results also confirm the intuition that limited resources should balance the radar sensing and multiuser broadcasting.
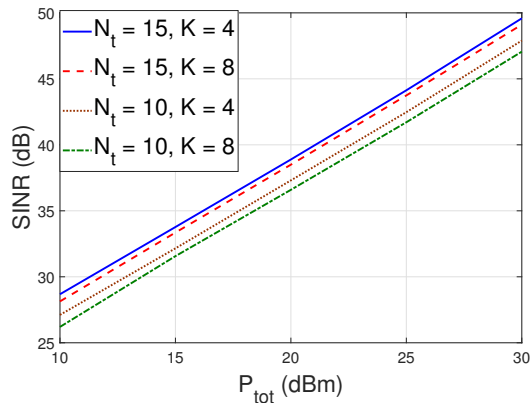
Fig. 10. The sensing SINR versus the total transmit power P_{tot} for $N_r = 10$, $R_i = 3$ dB, and different N_t and K.
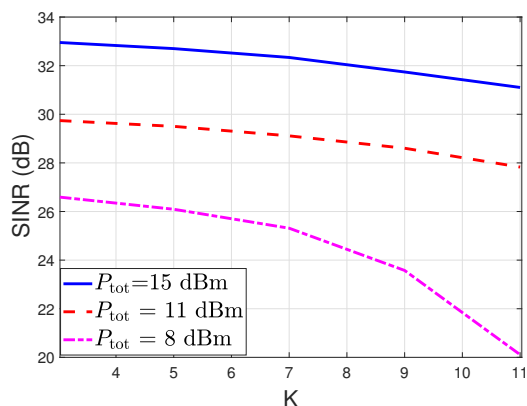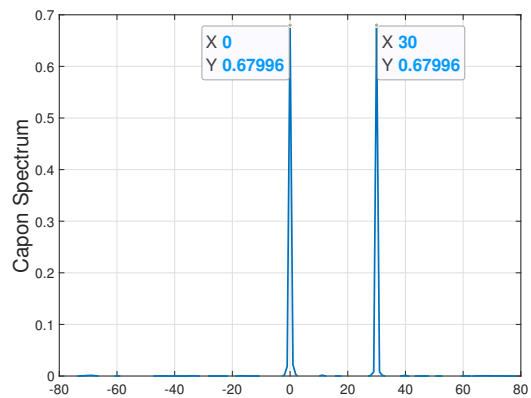

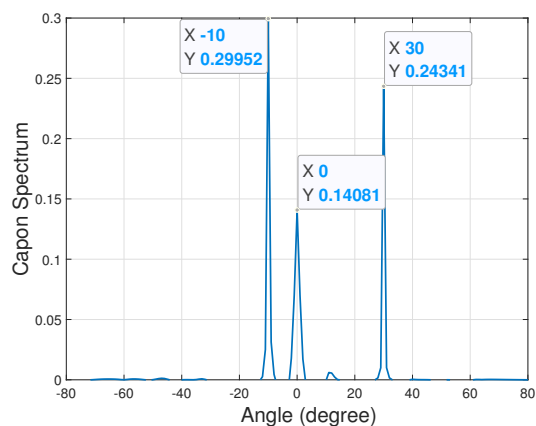Fig. 11. The sensing SINR versus the number of users K for $N_t = 15$, $N_r = 10$, $R_i = 5$ dB, and different P_{tot}.

(a)

(b)

Fig. 12. Capon spatial spectral estimates in presence of signal-dependent interference:(a) two targets with $\upsilon_1 = 0^o$ and $\upsilon_2 = 30^o$;(b) three targets with $\upsilon_1 = -10^o$, $\upsilon_2 = 0^o$, and $\upsilon_3 = 30^o$.

Fig. 10 illustrates the behavior of the sensing SINR at the radar receiver. Different from the signal independent interference case, the clutter interference originates from the transmit signal which certainly increases with increasing P_{tot}. However, through optimizing transmit beamforming and receiver, the clutter interference can be suppressed for improving the sensing SINR at the radar receiver. Therefore, simulation results show that the behavior of the sensing SINR at the radar receiver is similar to the signal-independent case. Moreover, the sensing SINR also increases with the increasing N_t and the decreasing K. This is because with the increasing N_t, more spatial DoF can be utilized for serving multiuser broadcasting and radar sensing. Accordingly, decreasing K reduces the spatial resources used for communication signal broadcasting, and then the corresponding spatial DoF used for radar sensing increases and the sensing SINR of the radar improves accordingly.

Fig. 11 shows the sensing SINR of the radar versus the number of users, K for different P_{tot}. With the increasing K, more resources should be utilized for communications due to the constraints of the SINR received at multiple users. Therefore, from Fig. 11, we observe that the sensing SINR decreases with the increasing K. Moreover, from Fig. 11, we can also

find that the reduction rate of the sensing SINR decreases with the increasing P_{tot}, since the increasing transmit power counteracts the adverse effect brought by increasing K on the sensing SINR at the radar receiver.

For measuring the radar sensing performance in the presence of signal-dependent interference, in Fig. 12, we consider different numbers of targets to plot the Capon spatial spectrum. Like the signal-independent interference, the Capon spectrum has narrow peaks only at the target angles, which validates the efficiency of our proposed Algorithm 3 in suppressing signal-dependent interference.

In Fig. 13, we consider the same vehicle-to-infrastructure communication scenario as Fig. 6 in cluttered environments. The angle tracking performance of EKF is illustrated in Fig. 13(a). Fig. 13(b) shows the real sensing SINR and the estimated one of PA during the tracking stage, where the clutter has the same parameters as the signal-independent interference in Fig. 6. Obviously, the imperfect angle estimation results in the performance degradation, but its degradation is slight. Therefore, the simulation results in Fig. 13 confirm the performance of our proposed DFRC precoder for tracking a moving target even in cluttered environments.
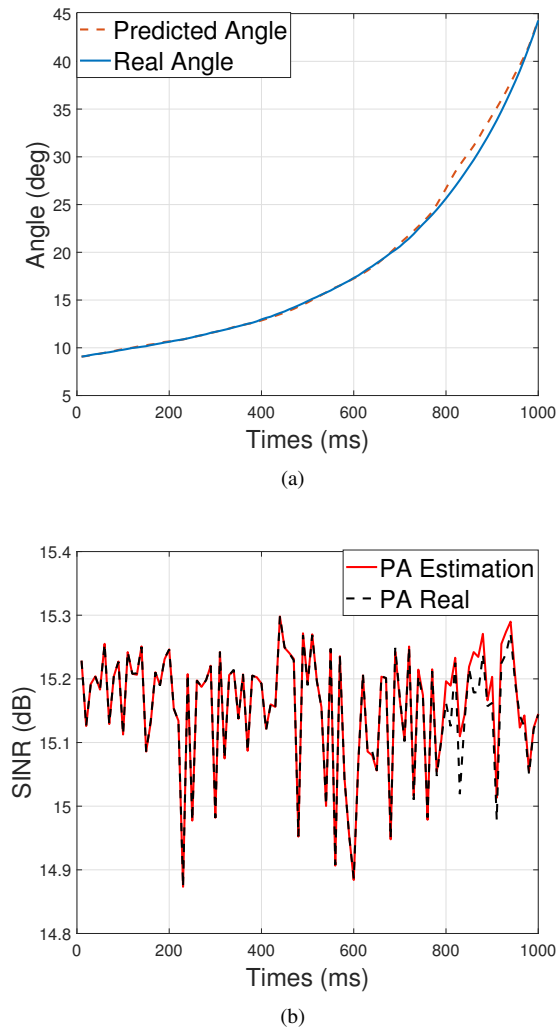
Fig. 13. The sensing SINR for the radar tracking scenario with $N_t = 15$, $N_r = 20$, and $K = 10$ in the presence of signal-dependent clutter: (a) Angle tracking performances of EKF; (b) Sensing SINR comparison

VI. CONCLUSIONS

In this paper, we have considered signal-independent interference and signal-dependent clutter to design the precoder of the MIMO-DFRC system for maximizing the sensing SINR at the radar receiver under the minimum SINR received at multiple communciation users and per-antenna power constraint. We have proposed distance-majorization induced algorithms to handle the nonconvexity of the objective function and per-antenna power constraint, which transformed the nonconvex design problem into a sequence of unconstrained convex problems whose optimal solutions can be obtained in closed form. Analytical results showed that compared with existing SDR-based approach, the complexity of our proposed algorithms is significantly lower. Besides, our simulation results confirmed the superior performance of our proposed algorithm, by comparing with the SDR-based approach. Therefore, the contribution of this work is to propose a novel algorithm for handling the nonconvex precoding optimization problem, which achieves better DFRC performance than the state-of-

the-art algorithm with a much lower computational complexity.

Some future research directions are outlined as follows. Firstly, this treatise assumes that the perfect channel state information (CSI) is available for optimizing DFRC precoder. However, we can only estimate imperfect CSI with the channel estimation technique in practical systems. Then, one of the open problems is to consider imperfect CSI to design efficient algorithms to optimize robust DFRC precoder. Secondly, this work does not consider the security of communication signals aided radar sensing. However, the increasing radiation power will make communication signals more vulnerable to eavesdropping attack. Therefore, it will be another problem how to design the DFRC precoder for radar sensing and secure communications.

APPENDIX A
PROOF OF THEOREM 1

In the proof, we only consider the case that $\sqrt{1 + \frac{1}{R_i}} r_i < ||\mathbf{f}_i||_2$. For notational brevity, we denote $\alpha_i \triangleq \sqrt{1 + \frac{1}{R_i}}$, $r_i \triangleq \mathbf{g}_{i,1}\bar{\mathbf{w}}$, and $\mathbf{f}_i \triangleq \bar{\mathbf{H}}_i\bar{\mathbf{w}} + \bar{\mathbf{b}}_i$. Accordingly, the projection of $(r_i, \mathbf{f}_i)$ onto the set of Ω can be formulated as the following optimization problem

$$\underset{\hat{r}_i(k), \hat{\mathbf{f}}_i(k)}{\text{minimize}} \ |\hat{r}_i(k) - r_i|^2 + \left\| \hat{\mathbf{f}}_i(k) - \mathbf{f}_i \right\|_2^2 \quad (34a)$$

$$\text{s.t.} \ \alpha_i \hat{r}_i(k) \geq ||\hat{\mathbf{f}}_i(k)||_2, \quad (34b)$$

where constraint (34b) defines the set of Ω_i.

It is easy to prove that the optimal solution of problem (34) satisfies the inequality constraint with equality. Its Lagrangian is given by

$$L\left(\hat{r}_i(k), \hat{\mathbf{f}}_i(k), \mu\right) = |\hat{r}_i(k) - r_i|^2 + \left\| \hat{\mathbf{f}}_i(k) - \mathbf{f}_i \right\|_2^2$$
$$+ \mu\left(||\hat{\mathbf{f}}_i(k)||_2^2 - \alpha_i \hat{r}_i(k)\right), \quad (35)$$

where μ is the dual variable. The analytical result of $\hat{r}_i(k)$ and $\hat{\mathbf{f}}_i(k)$ can be obtained from the KKT condition of problem (34), given by

$$\hat{r}_i(k) = r_i + \alpha_i \mu, \quad (36)$$

$$\hat{\mathbf{f}}_i(k) = \mathbf{f}_i - \mu\nu, \quad (37)$$

$$\alpha_i \hat{r}_i(k) = ||\hat{\mathbf{f}}_i(k)||_2, \quad (38)$$

where the subgradient $\nu \in \mathbb{C}^{2(N_t+1)\times 1}$ of $||\cdot||_2$ at $\hat{\mathbf{f}}_i(k)$ is given by [62, Theorem 28.2]

$$\nu = \hat{\mathbf{f}}_i(k)/||\hat{\mathbf{f}}_i(k)||_2, \qquad \text{if } \hat{\mathbf{f}}_i(k) \neq \mathbf{0}, \quad (39)$$

$$||\nu||_2 \leq 1, \qquad \text{if } \hat{\mathbf{f}}_i(k) = \mathbf{0}. \quad (40)$$

When $\hat{\mathbf{f}}_i(k) = \mathbf{0}$, we have $\hat{r}_i(k) = 0$. Therefore, assuming that $\hat{\mathbf{f}}_i(k) \neq \mathbf{0}$, we have $\hat{\mathbf{f}}_i(k) = \mathbf{f}_i - \mu\hat{\mathbf{f}}_i(k)/||\hat{\mathbf{f}}_i(k)||_2$. Denoting $\beta_i = 1 + \mu/||\hat{\mathbf{f}}_i(k)||_2$, we have $\mathbf{f}_i = \beta_i\hat{\mathbf{f}}_i(k)$ and $\mu = \beta_i||\hat{\mathbf{f}}_i(k)||_2 - ||\hat{\mathbf{f}}_i(k)||_2$.

Then, using (36), we have

$$\hat{r}_i(k) = r_i + \alpha_i\left(\beta_i||\hat{\mathbf{f}}_i(k)||_2 - ||\hat{\mathbf{f}}_i(k)||_2\right) \overset{(a)}{=} \frac{1}{\alpha_i}||\hat{\mathbf{f}}_i(k)||_2, \quad (41)$$

where equality (a) is due to condition (38). Accordingly, we have $r_i = \left(\frac{1}{\alpha_i} + \alpha_i - \alpha_i\beta_i\right)||\hat{\mathbf{f}}_i(k)||_2$ and $||\mathbf{f}_i||_2 = \frac{\beta_i r_i}{\frac{1}{\alpha_i} + \alpha_i - \alpha_i\beta_i}$, since $\mathbf{f}_i = \beta_i\hat{\mathbf{f}}_i(k)$. Therefore, we have

$$\beta_i = \frac{||\mathbf{f}_i||_2\left(\alpha_i + \frac{1}{\alpha_i}\right)}{r_i + \alpha_i||\mathbf{f}_i||_2}. \tag{42}$$

Besides, substituting (42) into (41), we have

$$\hat{r}_i(k) = \frac{[||\mathbf{f}_i||_2 + r_i/\alpha_i]^+}{\alpha_i + \frac{1}{\alpha_i}}, \tag{43}$$

where the operator $[\cdot]^+$ is used for guaranteeing the non-negativity of $\hat{r}_i(k)$.

Furthermore, since $\mu = \beta_i||\hat{\mathbf{f}}_i(k)||_2 - ||\hat{\mathbf{f}}_i(k)||_2$, we have

$$\mu = \left(\frac{||\mathbf{f}_i||_2\left(\alpha_i + \frac{1}{\alpha_i}\right)}{r_i + \alpha_i||\mathbf{f}_i||_2} - 1\right)||\hat{\mathbf{f}}_i(k)||_2 \tag{44}$$

$$\overset{(a)}{=} \frac{(||\mathbf{f}_i||_2/\alpha_i - r_i)}{\alpha_i + 1/\alpha_i}. \tag{45}$$

where equality (a) is due to $\mathbf{f}_i = \beta_i\hat{\mathbf{f}}_i(k)$ and (42).

Since $\mathbf{f}_i = \beta_i\hat{\mathbf{f}}_i(k)$ and $\beta_i \triangleq 1 + \frac{\mu}{||\hat{\mathbf{f}}_i(k)||_2}$, we have

$$\mathbf{f}_i = \hat{\mathbf{f}}_i(k)\left(1 + \frac{\mu}{||\hat{\mathbf{f}}_i(k)||_2}\right) \overset{(a)}{=} \hat{\mathbf{f}}_i(k)\left(1 + \frac{\mu/\alpha_i}{\hat{r}_i(k)}\right) \tag{46}$$

$$\overset{(b)}{=} \hat{\mathbf{f}}_i(k)\left(1 + \frac{1/\alpha_i(1/\alpha_i||\mathbf{f}_i||_2 - r_i)}{[||\mathbf{f}_i||_2 + 1/\alpha_i r_i]^+}\right), \tag{47}$$

where step (a) is due to (38) and step (b) is due to (43) and (45). Furthermore, from (47), we have

$$\hat{\mathbf{f}}_i(k) = \mathbf{f}_i\frac{[||\mathbf{f}_i||_2 + 1/\alpha_i r_i]^+}{[||\mathbf{f}_i||_2 + 1/\alpha_i r_i]^+ + 1/\alpha_i(1/\alpha_i||\mathbf{f}_i||_2 - r_i)}$$

$$\overset{(a)}{=} \mathbf{f}_i\frac{[||\mathbf{f}_i||_2 + 1/\alpha_i r_i]^+}{||\mathbf{f}_i||_2 + 1/\alpha_i^2||\mathbf{f}_i||_2}, \tag{48}$$

where equality (a) is due to the fact that $[||\mathbf{f}_i||_2 + 1/\alpha_i r_i]^+ = 0$ when $||\mathbf{f}_i||_2 + 1/\alpha_i r_i < 0$.

APPENDIX B
PROOF OF THEOREM 2

Defining $c_{1,i}(\bar{\mathbf{w}}) \triangleq \text{dist}\left([\mathbf{g}_{i,1}\bar{\mathbf{w}}; \bar{\mathbf{H}}_i\bar{\mathbf{w}} + \bar{\mathbf{b}}_i], \Omega_i\right)$, $c_2(\bar{\mathbf{w}}) \triangleq \text{dist}(\bar{\mathbf{w}}, \Xi)$, and $c_{3,i}(\bar{\mathbf{w}}) \triangleq |\mathbf{g}_{i,2}\bar{\mathbf{w}}|$, problem (12) can be equivalently reformulated as follows

$$\max_{\bar{\mathbf{w}}, v_i, \bar{\mathbf{y}}, r_i, \mathbf{f}_i} \bar{\mathbf{w}}^T\bar{\Theta}\bar{\mathbf{w}} \tag{49a}$$

$$\text{s.t.} c_{1,i}(\bar{\mathbf{w}})=0, c_2(\bar{\mathbf{w}})=0, c_{3,i}(\bar{\mathbf{w}})=0, 1 \leq i \leq K, (12c). \tag{49b}$$

In the following, we prove that Algorithm 1 converges to a KKT solution of problem (49). The KKT conditions of problem (49) are given as follows

$$\nabla_{\bar{\mathbf{w}}^*}\mathcal{L}\left(\bar{\mathbf{w}}^*, \varpi_{1,i}^*, \varpi_2^*, \varpi_{3,i}^*, \lambda^*\right) = \mathbf{0} \tag{50}$$

$$c_{1,i}(\bar{\mathbf{w}}^*)=0, c_2(\bar{\mathbf{w}}^*)=0, c_{3,i}(\bar{\mathbf{w}}^*)=0, 1 \leq i \leq K \tag{51}$$

$$(\bar{\mathbf{w}}^*)^T\bar{\mathbf{w}}^* \leq P_{\text{tot}} \tag{52}$$

$$\lambda^*\left((\bar{\mathbf{w}}^*)^T\bar{\mathbf{w}}^* - P_{\text{tot}}\right) = 0, \tag{53}$$

where

$$\mathcal{L}\left(\bar{\mathbf{w}}^*, \varpi_{1,i}^*, \varpi_2^*, \varpi_{3,i}^*, \lambda^*\right) = -\bar{\mathbf{w}}^T\bar{\Theta}\bar{\mathbf{w}} + \sum_{1 \leq i \leq K}\varpi_{1,i}^*c_{1,i}(\bar{\mathbf{w}}^*)$$

$$+\varpi_2^*c_2(\bar{\mathbf{w}}^*) + \sum_{1 \leq i \leq K}\varpi_{3,i}^*c_{3,i}(\bar{\mathbf{w}}^*) + \lambda^*\left((\bar{\mathbf{w}}^*)^T\bar{\mathbf{w}}^* - P_{\text{tot}}\right),$$

where $\varpi_{1,i}^*$, ϖ_2^*, $\varpi_{3,i}^*$, and λ^* are Lagrange multipliers associated with constraints in (49b). In the following, we exploit [53, Theorem 17.2] to prove that the solution obtained by the penalty method also satisfies conditions provided by Eqs. (50)-(53).

With the penalty method, equality constraints can be moved into the objective function as follows

$$\min_{\bar{\mathbf{w}}} -\bar{\mathbf{w}}^T\bar{\Theta}\bar{\mathbf{w}} + \frac{\rho}{2}\left(\sum_{1 \leq i \leq K}\left(c_{1,i}^2(\bar{\mathbf{w}}) + c_{3,i}^2(\bar{\mathbf{w}})\right) + c_2^2(\bar{\mathbf{w}})\right)$$

$$\text{s.t. } (12c). \tag{54}$$

Obviously, problem (54) is equivalent to problem (13). The Lagrangian associated with problem (54) is given by

$$L\left(\bar{\mathbf{w}}, \hat{\lambda}\right) \triangleq \frac{\rho}{2}\left(\sum_{1 \leq i \leq K}\left(c_{1,i}^2(\bar{\mathbf{w}}) + c_{3,i}^2(\bar{\mathbf{w}})\right) + c_2^2(\bar{\mathbf{w}})\right)$$

$$- \bar{\mathbf{w}}^T\bar{\Theta}\bar{\mathbf{w}} + \hat{\lambda}\left(\bar{\mathbf{w}}^T\bar{\mathbf{w}} - P_{\text{tot}}\right), \tag{55}$$

where $\hat{\lambda}$ is the Lagrange multiplier associated with constraint (12c). By differentiating $L\left(\bar{\mathbf{w}}, \hat{\lambda}\right)$, we have

$$\nabla_{\bar{\mathbf{w}}}L\left(\bar{\mathbf{w}}, \hat{\lambda}\right) \triangleq \Upsilon\left(\bar{\mathbf{w}}, \hat{\lambda}\right) = -2\bar{\Theta}\bar{\mathbf{w}} + \sum_{1 \leq i \leq K}\rho c_{1,i}(\bar{\mathbf{w}})\nabla_{\bar{\mathbf{w}}}c_{1,i}(\bar{\mathbf{w}})$$

$$+ 2\hat{\lambda}\bar{\mathbf{w}} + \sum_{1 \leq i \leq K}\rho c_{3,i}(\bar{\mathbf{w}})\nabla_{\bar{\mathbf{w}}}c_{3,i}(\bar{\mathbf{w}}) + \rho c_2(\bar{\mathbf{w}})\nabla_{\bar{\mathbf{w}}}c_2(\bar{\mathbf{w}}).$$

When $\Upsilon\left(\bar{\mathbf{w}}^*, \hat{\lambda}^*\right) \to 0$, with the inequality $||a|| - ||b|| \leq ||a + b||$, we have (56) at the top of the next page. Since the gradients $\nabla c_{1,i}(\bar{\mathbf{w}}^*)$, $\nabla c_2(\bar{\mathbf{w}}^*)$, and $\nabla c_{3,i}(\bar{\mathbf{w}}^*)$ are all linearly independent, we can conclude that $c_{1,i}(\bar{\mathbf{w}}^*) = 0$, $c_2(\bar{\mathbf{w}}^*) = 0$, and $c_{3,i}(\bar{\mathbf{w}}^*) = 0$, which satisfies condition (51).

In addition, since $\lim_{\rho \to +\infty} -2\bar{\Theta}\bar{\mathbf{w}} + \sum_{1 \leq i \leq K}\rho c_{1,i}(\bar{\mathbf{w}})\nabla_{\bar{\mathbf{w}}}c_{1,i}(\bar{\mathbf{w}}) + 2\lambda\bar{\mathbf{w}} + \sum_{1 \leq i \leq K}\rho c_{3,i}(\bar{\mathbf{w}})\nabla_{\bar{\mathbf{w}}}c_{3,i}(\bar{\mathbf{w}}) + \rho c_2(\bar{\mathbf{w}})\nabla_{\bar{\mathbf{w}}}c_2(\bar{\mathbf{w}}) = 0$, condition (50) holds when we set

$$\lim_{\rho \to +\infty}\rho c_{1,i}(\bar{\mathbf{w}}^*) = \varpi_{1,i}^*, 1 \leq i \leq K, \tag{57}$$

$$\lim_{\rho \to +\infty}\rho c_2(\bar{\mathbf{w}}^*) = \varpi_2^*, \tag{58}$$

$$\lim_{\rho \to +\infty}\rho c_{3,i}(\bar{\mathbf{w}}^*) = \varpi_{3,i}^*, 1 \leq i \leq K. \tag{59}$$

Besides, conditions (52) and (53) obviously hold, since $\hat{\lambda}$ is the Lagrange multiplier associated with constraint (12c).

Hence, as $\rho \to +\infty$, the KKT solution of problem (54) also satisfies the KKT condition of problem (49). Furthermore, we employ the majorization-minimization algorithm [54] to design Algorithm 1 that solves the convex approximation of problem (54), i.e., problem (15), iteratively. Then, since Algorithm 1 satisfies conditions in [54, eq. (2) and eq. (3)], we

$$\left\|\sum_{1\le i\le K}\left(c_{1,i}\left(\bar{\mathbf{w}}^*\right)\nabla_{\bar{\mathbf{w}}^*}c_{1,i}\left(\bar{\mathbf{w}}^*\right)+c_{3,i}\left(\bar{\mathbf{w}}^*\right)\nabla_{\bar{\mathbf{w}}^*}c_{3,i}\left(\bar{\mathbf{w}}^*\right)\right)+c_2\left(\bar{\mathbf{w}}^*\right)\nabla_{\bar{\mathbf{w}}^*}c_2\left(\bar{\mathbf{w}}^*\right)\right\|_2$$
$$\le\frac{1}{\rho}\left(\left\|\Upsilon\left(\bar{\mathbf{w}}^*,\hat{\lambda}^*\right)\right\|_2+\left\|2\lambda\bar{\mathbf{w}}^*-2\bar{\Theta}\bar{\mathbf{w}}^*\right\|_2\right)\overset{\rho\to+\infty}{\longrightarrow}0. \tag{56}$$

can conclude that Algorithm 1 converges to a KKT solution of problem (54), which also satisfies the KKT condition of problem (49). Besides, since problem (49) is equivalent to problem (12), the proof can be achieved.

APPENDIX C
BENCHMARK ALGORITHM: SDR-BASED ALGORITHM

We first introduce auxiliary variables $\Lambda_i\triangleq\mathbf{W}(:,i)\mathbf{W}^H(:,i)$ to reformulate the problem as the following semidefinite programming

$$\max_{\Lambda_i\in\mathbb{S}^+_{N_t\times N_t}}\sum_{i=1}^K\mathrm{Tr}\left(\Theta\Lambda_i\right) \tag{60a}$$

$$\text{s.t. }\frac{\mathbf{h}_i^H\Lambda_i\mathbf{h}_i}{\sum_{j\ne i}\mathbf{h}_i^H\Lambda_j\mathbf{h}_i+\sigma_i^2}\ge R_i,\ i=1,\ldots,K, \tag{60b}$$

$$\mathrm{diag}\left(\sum_{i=1}^K\Lambda_i\right)=\frac{P_{\text{tot}}}{N_t}\mathbf{I},\ i=1,\ldots,K, \tag{60c}$$

$$\mathrm{rank}\left(\Lambda_i\right)=1,\ i=1,\ldots,K. \tag{60d}$$

Following [33], we employ the penalty-based method to handle the rank constraint (60d). In particular, since when constraint (60d) holds, we have $||\Lambda_i||_*-||\Lambda_i||_2=0$. Then, when $\varsigma\to+\infty$, problem (60) is equivalent to the following problem

$$\max_{\mathbf{W}}\sum_{i=1}^K\mathrm{Tr}\left(\Theta\Lambda_i\right)-\varsigma\left(||\Lambda_i||_*-||\Lambda_i||_2\right)$$
$$\text{s.t. }\mathbf{h}_i^H\Lambda_i\mathbf{h}_i\ge R_i\sum_{j\ne i}\mathbf{h}_i^H\Lambda_j\mathbf{h}_i+\sigma_i^2,\ (60c). \tag{61}$$

However, its objective function is nonconvex due to $||\Lambda_i||_2$. By employing the successive convex approximation method [63], we approximate $||\Lambda_i||_2$ as $\bar{\Lambda}_i^k\triangleq-||\Lambda_i(k-1)||_2-\mathrm{Tr}\left(\mathbf{v}_{\max}\left(\Lambda_i(k-1)\right)\mathbf{v}_{\max}^H\left(\Lambda_i(k-1)\right)\left(\Lambda_i-\Lambda_i(k-1)\right)\right)$, where $\Lambda_i(k-1)$ is the solution obtained at the $(k-1)$th iteration [33]. Accordingly, a KKT solution of problem (61) can be obtained by solving a sequence of convex problems, given by

$$\max_{\mathbf{W}}\sum_{i=1}^K\mathrm{Tr}\left(\Theta\Lambda_i\right)-\varsigma\bar{\Lambda}_i^k,\ \text{s.t. (61).} \tag{62}$$

Algorithm 4 summarizes the benchmark algorithm.

Algorithm 4 Benchmark Algorithm for Solving Problem (11)

1: Initialize ς, $c=1.5$, $\varsigma_{\max}=10^4$, $\Lambda_i(0)\in\mathbb{R}^{N_t\times N_t}$, the convergence tolerance $\epsilon\ll1$, $\phi\ll1$ and $k=1$.
2: **Repeat**
3: Solving problem (62) and obtaining $\Lambda_i(k)$,
4: $\varsigma=\min\left(c\varsigma,\varsigma_{\max}\right)$
5: $k=k+1$,
6: **Until** $\bar{\Lambda}_i^k\le\epsilon$ and the objective function value improvement is less than ϕ.

REFERENCES

[1] J. A. Zhang, M. L. Rahman, K. Wu, X. Huang, Y. J. Guo, S. Chen, and J. Yuan, "Enabling joint communication and radar sensing in mobile networks—a survey," *IEEE Commun. Surv. Tutor.*, vol. 24, no. 1, pp. 306–345, Oct. 2022.

[2] Z. Wei, F. Liu, C. Masouros, N. Su, and A. P. Petropulu, "Toward multi-functional 6G wireless networks: Integrating sensing, communication, and security," *IEEE Commun. Mag.*, vol. 60, no. 4, pp. 65–71, Apr. 2022.

[3] J. A. Zhang, F. Liu, C. Masouros, R. W. Heath, Z. Feng, L. Zheng, and A. Petropulu, "An overview of signal processing techniques for joint communication and radar sensing," *IEEE J. Sel. Top. Signal Proces.*, vol. 15, no. 6, pp. 1295–1315, Nov. 2021.

[4] F. Liu, Y. Cui, C. Masouros, J. Xu, T. X. Han, Y. C. Eldar, and S. Buzzi, "Integrated sensing and communications: Toward dual-functional wireless networks for 6G and beyond," *IEEE J. Sel. Areas Commun.*, vol. 40, no. 6, pp. 1728–1767, Jun. 2022.

[5] S. Li, W. Yuan, C. Liu, Z. Wei, J. Yuan, B. Bai, and D. W. K. Ng, "A novel ISAC transmission framework based on spatially-spread orthogonal time frequency space modulation," *IEEE J. Sel. Areas Commun.*, vol. 40, no. 6, pp. 1854–1872, Jun. 2022.

[6] A. R. Chiriyath, B. Paul, and D. W. Bliss, "Radar-communications convergence: Coexistence, cooperation, and co-design," *IEEE Trans. Cogn. Commun. Netw.*, vol. 3, no. 1, pp. 1–12, Mar. 2017.

[7] Y. Cui, V. Koivunen, and X. Jing, "Precoder and decoder co-designs for radar and communication spectrum sharing," *Sensors*, vol. 22, no. 7, 2022. [Online]. Available: https://www.mdpi.com/1424-8220/22/7/2619

[8] R. M. Mealey, "A method for calculating error probabilities in a radar communication system," *IEEE Trans. Space Electron. Telem.*, vol. 9, no. 2, pp. 37–42, Jun. 1963.

[9] Y. Chen and X. Gu, "Time allocation for integrated bi-static radar and communication systems," *IEEE Commun. Lett.*, vol. 25, no. 3, pp. 1033–1036, Mar. 2021.

[10] J. Liu, K. V. Mishra, and M. Saquib, "Co-designing statistical MIMO radar and in-band full-duplex multi-user MIMO communications," *arXiv preprint arXiv:2006.14774*, 2022.

[11] ——, "Distributed beamforming for joint radar-communications," in *2022 IEEE 12th Sensor Array and Multichannel Signal Processing Workshop (SAM)*, 2022, pp. 151–155.

[12] F. Wang and H. Li, "Power allocation for coexisting multicarrier radar and communication systems in cluttered environments," *IEEE Trans. Signal Process.*, vol. 69, pp. 1603–1613, Feb. 2021.

[13] F. Liu, C. Masouros, A. Li, T. Ratnarajah, and J. Zhou, "MIMO radar and cellular coexistence: A power-efficient approach enabled by interference exploitation," *IEEE Trans. Signal Process.*, vol. 66, no. 14, pp. 3681–3695, May 2018.

[14] E. Grossi, M. Lops, and L. Venturino, "Energy efficiency optimization in radar-communication spectrum sharing," *IEEE Trans. Signal Process.*, vol. 69, pp. 3541–3554, May 2021.

[15] M. Roberton and E. Brown, "Integrated radar and communications based on chirped spread-spectrum techniques," in *IEEE MTT-S International Microwave Symposium Digest*, vol. 1, Philadelphia, PA, USA, Jun. 2003, pp. 611–614.

[16] D. Ciuonzo, A. De Maio, G. Foglia, and M. Piezzo, "Intrapulse radar-embedded communications via multiobjective optimization," *IEEE Trans. Aerosp. Electron. Syst.*, vol. 51, no. 4, pp. 2960–2974, Oct. 2015.

[17] Y. Gu, L. Zhang, Y. Zhou, and Q. Zhang, "Embedding communication symbols into radar waveform with orthogonal FM scheme," *IEEE Sens. J.*, vol. 18, no. 21, pp. 8709–8719, Nov. 2018.

[18] R. Liu, M. Li, Q. Liu, and A. L. Swindlehurst, "Dual-functional radar-communication waveform design: A symbol-level precoding approach," *IEEE J. Sel. Top. Signal Proces.*, vol. 15, no. 6, pp. 1316–1331, Nov. 2021.

[19] A. Zhang, M. L. Rahman, X. Huang, Y. J. Guo, S. Chen, and R. W. Heath, "Perceptive mobile networks: Cellular networks with radio vision via joint communication and radar sensing," *IEEE Veh. Technol. Mag.*, vol. 16, no. 2, pp. 20–30, Jun. 2021.

[20] C. Sturm and W. Wiesbeck, "Waveform design and signal processing aspects for fusion of wireless communications and radar sensing," *Proc. of the IEEE*, vol. 99, no. 7, pp. 1236–1259, Jul. 2011.

[21] R. Liu, M. Li, Q. Liu, and A. L. Swindlehurst, "Joint waveform and filter designs for STAP-SLP-based MIMO-DFRC systems," *IEEE J. Sel. Areas Commun.*, vol. 40, no. 6, pp. 1918–1931, Jun. 2022.

[22] N. Su, F. Liu, Z. Wei, Y.-F. Liu, and C. Masouros, "Secure dual-functional radar-communication transmission: Exploiting interference for resilience against target eavesdropping," *IEEE Trans. Wirel. Commun.*, pp. 1–15, Mar. 2022.

[23] N. Su, F. Liu, and C. Masouros, "Secure radar-communication systems with malicious targets: Integrating radar, communications and jamming functionalities," *IEEE Trans. Wirel. Commun.*, vol. 20, no. 1, pp. 83–95, Jan. 2021.

[24] F. Liu, C. Masouros, A. P. Petropulu, H. Griffiths, and L. Hanzo, "Joint radar and communication design: Applications, state-of-the-art, and the road ahead," *IEEE Trans. Commun.*, vol. 68, no. 6, pp. 3834–3862, Jun. 2020.

[25] F. Liu, Y.-F. Liu, A. Li, C. Masouros, and Y. C. Eldar, "Cramér-Rao bound optimization for joint radar-communication beamforming," *IEEE Trans. Signal Process.*, vol. 70, pp. 240–253, Jan. 2022.

[26] F. Liu, C. Masouros, T. Ratnarajah, and A. Petropulu, "On range sidelobe reduction for dual-functional radar-communication waveforms," *IEEE Wireless Commun. Lett.*, vol. 9, no. 9, pp. 1572–1576, Sept. 2020.

[27] F. Liu, L. Zhou, C. Masouros, A. Li, W. Luo, and A. Petropulu, "Toward dual-functional radar-communication systems: Optimal waveform design," *IEEE Trans. Signal Process.*, vol. 66, no. 16, pp. 4264–4279, Aug. 2018.

[28] Z. Zhang, Q. Chang, F. Liu, and S. Yang, "Dual-functional radar-communication waveform design: Interference reduction versus exploitation," *IEEE Commun. Lett.*, vol. 26, no. 1, pp. 148–152, Jul. 2022.

[29] L. Chen, F. Liu, W. Wang, and C. Masouros, "Joint radar-communication transmission: A generalized pareto optimization framework," *IEEE Trans. Signal Process.*, vol. 69, pp. 2752–2765, May. 2021.

[30] X. Liu, T. Huang, N. Shlezinger, Y. Liu, J. Zhou, and Y. C. Eldar, "Joint transmit beamforming for multiuser MIMO communications and MIMO radar," *IEEE Trans. Signal Process.*, vol. 68, pp. 3929–3944, Jun. 2020.

[31] X. Liu, T. Huang, and Y. Liu, "Transmit design for joint MIMO radar and multiuser communications with transmit covariance constraint," *IEEE J. Sel. Areas Commun.*, vol. 40, no. 6, pp. 1932–1950, Mar. 2022.

[32] C. Xu, B. Clerckx, S. Chen, Y. Mao, and J. Zhang, "Rate-splitting multiple access for multi-antenna joint radar and communications," *IEEE J. Sel. Top. Signal Proces.*, vol. 15, no. 6, pp. 1332–1347, Nov. 2021.

[33] X. Mu, Y. Liu, L. Guo, J. Lin, and L. Hanzo, "NOMA-aided joint radar and multicast-unicast communication systems," *IEEE J. Sel. Areas Commun.*, vol. 40, no. 6, pp. 1978–1992, Jun. 2022.

[34] C. Ding, J.-B. Wang, H. Zhang, M. Lin, and G. Y. Li, "Joint MIMO precoding and computation resource allocation for dual-function radar and communication systems with mobile edge computing," *IEEE J. Select. Areas Commun.*, vol. 40, no. 7, pp. 2085–2102, Jul. 2022.

[35] J. Johnston, L. Venturino, E. Grossi, M. Lops, and X. Wang, "MIMO OFDM dual-function radar-communication under error rate and beampattern constraints," *IEEE J. Sel. Areas Commun.*, vol. 40, no. 6, pp. 1951–1964, Jun. 2022.

[36] L. Chen, Z. Wang, Y. Du, Y. Chen, and F. R. Yu, "Generalized transceiver beamforming for DFRC with MIMO radar and MU-MIMO communication," *IEEE J. Sel. Areas Commun.*, vol. 40, no. 6, pp. 1795–1808, Jun. 2022.

[37] Z. Cheng and B. Liao, "QoS-aware hybrid beamforming and DOA estimation in multi-carrier dual-function radar-communication systems," *IEEE J. Select. Areas Commun.*, vol. 40, no. 6, pp. 1890–1905, Jun. 2022.

[38] Z. He, W. Xu, H. Shen, Y. Huang, and H. Xiao, "Energy efficient beamforming optimization for integrated sensing and communication," *IEEE Wireless Commun. Lett.*, vol. 11, no. 7, pp. 1374–1378, Jul. 2022.

[39] M. F. Keskin, V. Koivunen, and H. Wymeersch, "Limited feedforward waveform design for OFDM dual-functional radar-communications," *IEEE Trans. Signal Process.*, vol. 69, pp. 2955–2970, Apr. 2021.

[40] Z. He, W. Xu, S. Hong, D. W. K. Ng, E. Y. C., and Y. Xiaohu, "Full-duplex communication for ISAC: Joint beamforming and power optimization," *arXiv preprint arXiv:2211.00229*, 2022.

[41] J. Pritzker, J. Ward, and Y. C. Eldar, "Transmit precoder design approaches for dual-function radar-communication systems," *arXiv preprint arXiv:2203.09571*, 2022.

[42] K. L. Keys, H. Zhou, and K. Lange, "Proximal distance algorithms: Theory and practice," *Journal of Machine Learning Research*, vol. 20, pp. 1–38, Jul. 2019.

[43] J. Li, J. Guerci, and L. Xu, "Signal waveform's optimal-under-restriction design for active sensing," *IEEE Signal Process. Lett.*, vol. 13, no. 9, pp. 565–568, Sept. 2006.

[44] E. Grossi, M. Lops, and L. Venturino, "Joint design of surveillance radar and MIMO communication in cluttered environments," *IEEE Trans. Signal Process.*, vol. 68, pp. 1544–1557, Feb. 2020.

[45] G. Cui, H. Li, and M. Rangaswamy, "MIMO radar waveform design with constant modulus and similarity constraints," *IEEE Trans. Signal Process.*, vol. 62, no. 2, pp. 343–353, Jan. 2014.

[46] Z. Cheng, B. Liao, Z. He, J. Li, and J. Xie, "Joint design of the transmit and receive beamforming in MIMO radar systems," *IEEE Trans. Veh. Technol.*, vol. 68, no. 8, pp. 7919–7930, Aug. 2019.

[47] K. Shen, W. Yu, L. Zhao, and D. P. Palomar, "Optimization of MIMO device-to-device networks via matrix fractional programming: A minorization–maximization approach," *IEEE/ACM Trans. Netw.*, vol. 27, no. 5, pp. 2164–2177, Oct. 2019.

[48] Z. Cheng, Z. He, and B. Liao, "Hybrid beamforming for multi-carrier dual-function radar-communication system," *IEEE Trans. Cogn. Commun. Netw.*, vol. 7, no. 3, pp. 1002–1015, Mar. 2021.

[49] X. He and L. Huang, "Joint MIMO communication and MIMO radar under different practical waveform constraints," *IEEE Trans. Veh. Technol.*, vol. 69, no. 12, pp. 16 342–16 347, Dec. 2020.

[50] Z.-q. Luo, W.-k. Ma, A. M.-c. So, Y. Ye, and S. Zhang, "Semidefinite relaxation of quadratic optimization problems," *IEEE Signal Process. Mag.*, vol. 27, no. 3, pp. 20–34, Mar. 2010.

[51] S. Boyd and L. Vandenberghe, *Convex Optimization*. Cambridge, U.K.: Cambridge University Press, 2004.

[52] D. Bertsekas, *Nonlinear Programming, 2nd ed*. Belmont, MA, USA: Athena Scientific, 1999.

[53] J. Nocedal and S. J. Wright, *Numerical Optimization, 2nd*. NY, USA: Springer, 2006.

[54] Y. Sun, P. Babu, and D. P. Palomar, "Majorization-minimization algorithms in signal processing, communications, and machine learning," *IEEE Trans. Signal Process.*, vol. 65, no. 3, pp. 794–816, Feb. 2017.

[55] Q. Shi, M. Hong, X. Gao, E. Song, Y. Cai, and W. Xu, "Joint source-relay design for full-duplex MIMO AF relay systems," *IEEE Trans. Signal Process.*, vol. 64, no. 23, pp. 6118–6131, Dec. 2016.

[56] Z. Lu and Y. Zhang, "Penalty decomposition methods for rank minimization," *Optim. Methods Softw.*, vol. 30, no. 3, p. 531–558, May. 2015.

[57] X. Zhang, *Matrix Analysis and Applications*. Second Edition. Beijing, China: Tsinghua University Press, 2013.

[58] I. Pólik and T. Terlaky, *Interior Point Methods for Nonlinear Optimization*. Berlin, Heidelberg: Springer Berlin Heidelberg, 2010, pp. 215–276.

[59] Y. Yang, M. Pesavento, Z.-Q. Luo, and B. Ottersten, "Inexact block coordinate descent algorithms for nonsmooth nonconvex optimization," *IEEE Trans. Signal Process.*, vol. 68, pp. 947–961, Dec. 2020.

[60] L. Xu, J. Li, and P. Stoica, "Target detection and parameter estimation for mimo radar systems," *IEEE Trans. Aerosp. Electron. Syst.*, vol. 44, no. 3, pp. 927–939, Jul. 2008.

[61] F. Liu, W. Yuan, C. Masouros, and J. Yuan, "Radar-assisted predictive beamforming for vehicular links: Communication served by sensing," *IEEE Trans. Wireless Commun.*, vol. 19, no. 11, pp. 7704–7719, Aug. 2020.

[62] R. T. Rockafellar, *Convex Analysis*. Princeton, NJ: Princeton University Press, 1970.

[63] M. Hong, Q. Li, and Y.-F. Liu, "Decomposition by successive convex approximation: A unifying approach for linear transceiver design in heterogeneous networks," *IEEE Trans. Wireless Commun.*, vol. 15, no. 2, pp. 1377–1392, Feb. 2016.